International Journal of Nanomedicine

Dovepress
Taylor & Francis Group

Open Access Full Text Article

ORIGINAL RESEARCH

Design and Optimization of Trastuzumab-Functionalized Nanolipid Carriers for Targeted Capecitabine Delivery: Anti-Cancer Effectiveness Evaluation in MCF-7 and SKBR3 Cells

Shubhashree Das[1], Bhabani Sankar Satapathy[2], Gurudutta Pattnaik[1], Sovan Pattanaik[3], Yahya Alhamhoom[4], Mohamed Rahamathulla[4], Mohammed Muqtader Ahmed[5], Ismail Pasha[6]

[1]Department of Pharmaceutics, School of Pharmacy and Life Sciences, Centurion University of Technology and Management, Odisha, India; [2]Department of Pharmaceutics, GITAM School of Pharmacy, GITAM Deemed to Be University, Hyderabad Campus, Telangana, India; [3]Department of Pharmaceutical Chemistry, School of Pharmaceutical Sciences, Siksha O Anusandhan Deemed to be University, Bhubaneswar, Odisha, India; [4]Department of Pharmaceutics, College of Pharmacy, King Khalid University, Al Faraa, Abha, 62223, Saudi Arabia; [5]Department of Pharmaceutics, College of Pharmacy, Prince Sattam bin Abdul Aziz University, Al Kharj, 11942, Saudi Arabia; [6]Department of Pharmacology, Orotta College of Medicine and Health Science, Asmara, Eritrea

Correspondence: Gurudutta Pattnaik, School of Pharmacy and Life Sciences, Centurion University of Technology and Management, Odisha, India, Email gurudutta.pattnaik@cutm.ac.in; Ismail Pasha, Department of Pharmacology, Orotta college of medicine and Health Science, Asmara, Eritrea, Email ismail.orotta@gmail.com

Background: Breast cancer remains a leading cause of cancer-related mortality in women globally. The main purpose of the research to develop, optimise and characterise a trastuzumab (TZ)-functionalized nanolipid carrier (NCs) encapsulating capecitabine, as a targeted strategy to breast cancer cells, to enhance therapeutic efficacy and reduce the severe side effects associated with conventional chemotherapy.

Methods: Capecitabine encapsulated NCs (CBNCs) were prepared by thin-film hydration technique, optimized by Box-Behnken design. The optimized formulation CBNCs were subsequently conjugated with TZ by using EDC-NHS chemistry. The prepared formulations of NCs were evaluated by FTIR, DSC, XRD, FESEM, TEM, AFM, drug loading, entrapment efficiency, average particle size, PDI, zeta potential, in vitro drug release. The successful surface conjugation of TZ was tested by BCA assay and SDS-PAGE analysis. In vitro targeting efficiency and cytotoxicity initially tested in MCF-7 cells (HER2-low expressing) and subsequently validated in SKBR3 cells (HER2-overexpressing) to confirm receptor-mediated uptake and specificity.

Results: Optimized CBNCs were found spherical, nanosized (194.6 nm), with a zeta potential −25.55 mV for CBNCs, which increased to –57.76 mV upon TZ conjugation. The formulation showed 8.5% drug loading capacity and 84.26% drug release over 72 h. FTIR and DSC showed compatibility of drug and lipid components with no major shifting in characteristic peaks. TEM and AFM confirmed formation of stable, spherical discrete nanostructures. TZ conjugation showed minor alternation in average size/surface charge/morphology/texture. Successful TZ conjugation onto CBNCs was confirmed by BCA assay and SDS-PAGE. Fluorescence microscopy confirmed successful cellular internalization. MTT assay on SKBR3 cells demonstrated significantly higher cytotoxicity for TZ-CBNCs compared to CBNCs and free drug, thereby validating the HER2-specific targeting effect beyond preliminary results obtained in MCF-7 cells.

Conclusion: In view of the desired physicochemical properties, controlled drug release, and in vitro anticancer effectiveness, further in vivo investigations should be prioritized to validate its clinical application in HER2-positive breast cancer treatment. Nonetheless, the use of HER2-low MCF-7 cells in early assays highlights the importance of complementary validation in HER2-overexpressing models, as addressed by SKBR3 testing in this study.

Keywords: nanolipid carrier, trastuzumab, capecitabine, breast cancer, MTT assay

Received: 30 May 2025
Accepted: 25 September 2025
Published: 3 October 2025

Graphical Abstract

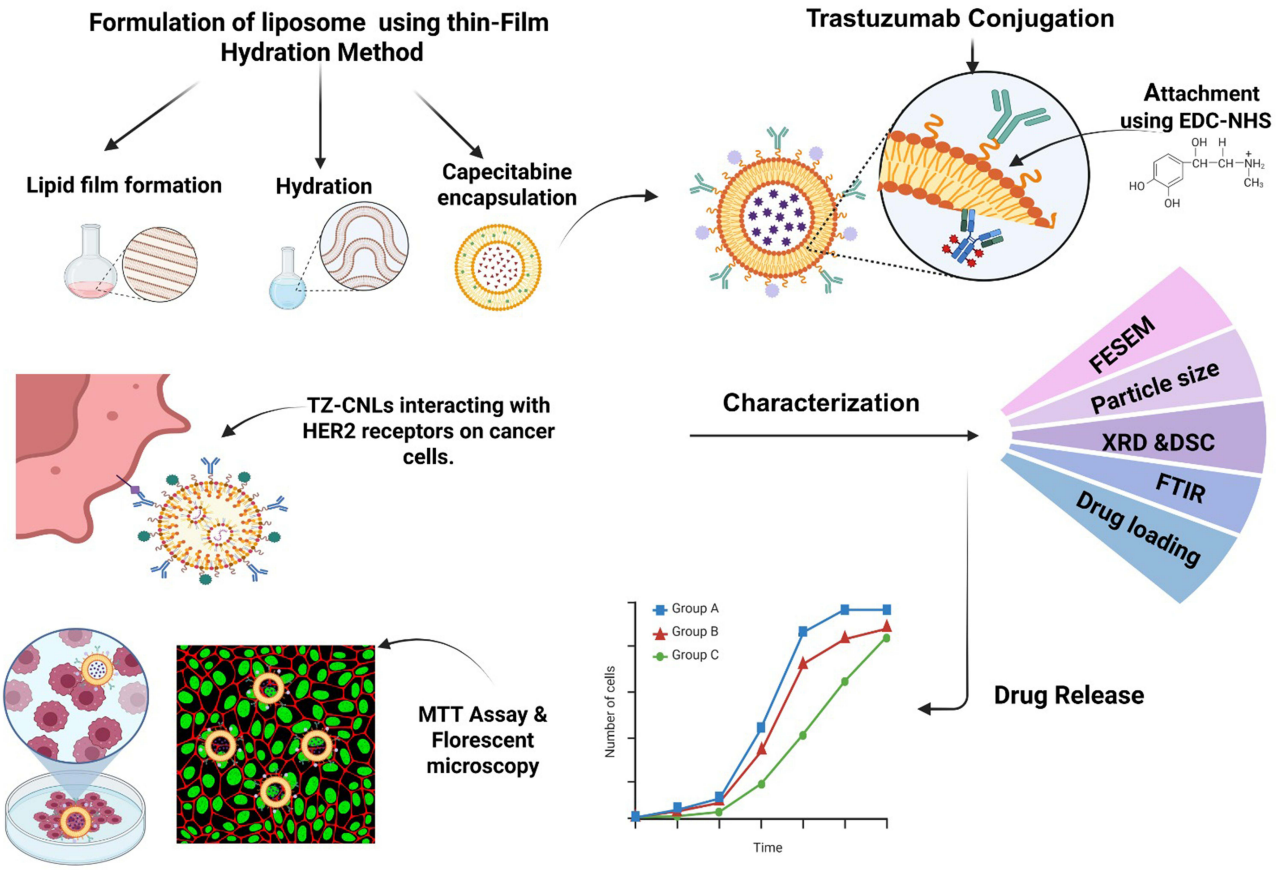

Introduction

Breast cancer is a prevalent and life-threatening disease in women, responsible for a substantial proportion of cancer deaths.[1,2] Especially, human epidermal growth factor receptor 2 (HER2)-positive breast cancers represent roughly 15–20% of all diagnosed cancer cases across the globe.[3–5] The HER2 receptor has been identified as one of the crucial receptors in the growth and proliferation of neoplastic cells, and its elevated expression is often linked to malignant progression of breast cancer.[6,7] Present treatment modalities including combination of radiation, surgery, chemotherapy, antibiotic therapy have often found insufficient to resist metastasis. Further, patients having breast cancer frequently develop tolerance towards chemotherapy.[8] The unbearable adverse effects of conventional chemo drugs too pose another challenge to complete the scheduled regimen. In this context, breast cancer cell-specific targeted delivery of anticancer drugs is considered alternative, hopeful approach to improve treatment outcome; side by side to check indiscriminate drug accumulation at non-cancerous/healthy tissue. Such active targeting approach mediated by antibodies, aptamers, peptides, etc. selectively target the cancer cells, resulting in more effective tumor growth inhibition.[9,10]

Trastuzumab (TZ) is an established antibody, that primarily works by blocking the growth of cancerous cells that overexpress HER2, making it a significant modality towards treatment of breast cancer.[11,12] Drug carriers functionalized with TZ thus can be specifically directed towards cancer cells, subsiding off-target drug loss and bizarre adverse effects. Capecitabine (CB) is an oral chemotherapeutic medication that disrupts DNA synthesis, resulting in cellular apoptosis. Nonetheless, the major drawback of capecitabine-based therapy lies in its high dose, poor bioavailability and off-target effects; resulting in sub-standard treatment effects.[6] Combination of CB with TZ has demonstrated a favourable synergistic strategy resulting in enhanced therapeutic outcomes in breast cancer.[13] Furthermore, evidence suggests that

incorporating CB to standard chemotherapy regimens ameliorated overall survival in patients with advanced breast cancer.[14] Ongoing research is exploring the potential of CB in combination with other targeted therapies too to achieve desired treatment outcomes and to improve quality of life in patients post treatment.[15]

Nanodrug carriers like nanoliposomes, polymeric nanoparticles, polymeric micelles, solid-lipid nanoparticles, dendrimers, niosomes, metallic nanocarriers etc., have opened promising avenues to modulate therapeutic effects of conventional chemotherapy.[16] Furthermore, these nanodrug carriers can be modified with receptor-specific ligands (*viz*. antibodies, peptides, aptamers, etc.) on their surface to improve targeting and bioavailability.[17–21] Among various nanodrug carriers, lipid nanocarrier-based formulations, *viz.*, nanoliposomes, solid-lipid nanocarriers, etc., are the scalable formulation technology. Ligand-modified nanoliposomes can target specific tumour cells, release drugs slowly over time, reduce drug-related toxicity, and improve the stability of the loaded medication(s).[22,23] Owing to their architectural uniqueness, cell-mimicking features, non-immunogenic nature, ability to encapsulate both hydrophilic and lipophilic entities, facile method of production, easy surface manipulation, sustained drug release property, lipid nanocarriers have now being widely investigated across formulation development fraternity to target breast cancer.[24]

In this context, the work aims to fabricate optimized TZ-functionalized nanolipid carriers loaded with capecitabine (TZ-CBNCs) as a targeting nanomodality against HER2-positive breast cancer. Experimental CBNCs were designed utilizing the Box-Behnken design technique to choose the optimized formulation/process parameters for scalable production of CBNCs. The optimized CBNCs were characterized by surface morphology, texture, average size, surface charge, and loading efficiency, followed by conjugation with TZ and further characterization. In vitro anticancer effectiveness of CBNCs/TZ-CBNCs was carried out by MTT and fluorescence microscopy against selected breast cancer cell lines.

Though recent studies have documented the potentiality of CB-loaded nanocarriers against breast cancers; however, the present study holds its own uniqueness and is not a mere repetition of any such similar reports. Singh et al (2020) designed tumor-homing peptide-conjugated liposomes for the targeted delivery of CB for breast carcinoma.[25] Mondal et al (2019) developed CD-340 antibody-conjugated PLGA nanoparticles loaded with doxorubicin, which demonstrated enhanced tumor targeting, apoptosis induction, and reduced cardiotoxicity in breast cancer models.[2] In another recent study by Kumar et al, trastuzumab-conjugated cationic liposomes co-delivering paclitaxel and ABCB1-siRNA were designed, which exhibited enhanced cellular uptake, superior tumor distribution, and improved therapeutic efficacy in HER2-positive breast cancer models.[26] However, design, fabrication and evaluation of TZ-functionalized optimized nanolipid carriers for targeted delivery CB was not reported elsewhere. Further, the work involves testing of anticancer effectiveness of the TZ-CBNCs in MCF-7 and SKBR3 to rationalize the HER2 targeting efficiency. Overall, the work highlights a targeted approach to enhance selective cytotoxicity and cellular uptake of CB through TZ-mediated targeting in HER2-positive breast cancer cells in vitro.

Materials and Methods

Materials

An additional sample of CB was bought from Cipla Ltd. (India), Mumbai, Maharashtra. Soya α-lecithin (SLT) was acquired from Nandini Lifesciences Pvt. Ltd., which is situated in Mumbai, India. E Merck Ltd. in Mumbai, India, provided cholesterol (CHT). Qualigens Fine Chemicals in Mumbai, India, supplied Butylated hydroxytoluene (BHT). TZ (marketed as Eleftha by Intas Pharmaceuticals) was obtained from the SUM Hospital pharmacy in Odisha, India. Avanti Polar Lipids, Inc. in Alabaster, AL, USA provided DSPE-PEG (2000)-COOH. The US-based Sigma Aldrich was the vendor for EDC and NHS. Sigma-Aldrich Co. (Bangalore, India) sold fluorescein isothiocyanate (FITC). All the extra chemicals in use were of analytical grade.

Cell Culture

The National Centre for Cell Science in Pune, India, is where the MCF-7 cells (weakly express HER2) and SKBR-3 cells (overexpress HER2) were purchased. Dulbecco's Modified Eagle Medium (for MCF-7 cells) and McCoy's 5A media (for SKBR-3 cells) supported the cell line's growth. Cells were cultivated in an appropriate growth medium at 37 °C in

a humidified incubator containing 5% CO_2 (CB160, Binder, Tuttlingen, Germany). The medium was enriched with 10% fetal bovine serum (FBS; Sigma-Aldrich Co), along with 100 U/mL penicillin and 100 U/mL streptomycin.

Methodology

Design of Experiment

Several parameters were checked before beginning the optimization process for the production of CBNCs. These factors included the ratio of the drug to lipids, the sonication duration, the hydration time, and the concentration of soy lecithin and cholesterol. Among that, three independent parameters were chosen for the Box-Behnken design (Design Expert® software version 13), and their impact on the formulation characteristics of CBNCs was then examined. A three-level, three-factor experimental framework with 15 trials was utilized to optimize the formulation variables in the nanoformulations.[27,28]

The amount of cholesterol (designated as X1), the centrifugation speed (designated as X2), and the sonication time (designated as X3) were the independent variables used for this research. Particle size (Y1), entrapment efficiency (Y2), and drug loading (Y3) were the dependent variables that were assessed in this study, as shown in Table 1. In this study, HOOC-DSPE-PEG-2000 and TZ were not incorporated into the design matrix, as a stepwise optimization strategy was adopted. Initially, the core formulation parameters (cholesterol concentration, centrifugation speed, and sonication time) were systematically optimized to ensure favorable physicochemical characteristics and drug-loading efficiency. Subsequent surface modification with HOOC-DSPE-PEG-2000 and TZ was performed only on the optimized base formulation to achieve targeted delivery, thereby minimizing potential confounding effects during the primary formulation optimization stage.

The ranges and levels of the selected variables were established based on preliminary optimization trials, insights from published literature, and practical considerations related to formulation feasibility. Specifically, cholesterol concentration was varied within a window that maintained an appropriate balance between membrane rigidity and entrapment efficiency. The centrifugation speed was adjusted to enable efficient vesicle integrity, and the sonication duration was selected to achieve effective size reduction without inducing structural disruption. Collectively, these ranges define a rational and experimentally relevant domain suitable for robust modeling using the Box–Behnken approach.[27,28]

Development of Capecitabine-Loaded Nanolipid Carrier (CBNCs)

CBNCs were developed using the conventional lipid layer hydration technique, following optimized parameters. CB, SL, HOOC-DSPE-PEG-2000, BHT, and CHT were measured and added in a 250 mL round-bottom flask before being rapidly agitated to dissolve in chloroform. A concentration level of 1% (w/v) BHT, which inhibits lipid oxidation, was also present in this mixture. A Rotavap suoerfit, PBU-6, Mumbai, India, a vacuum evaporator with a circulating water bath, was used to hold the sample. At 40 °C and 100 rpm, it was spinning. After the solvent evaporated, the inside surfaces of the round-bottom flask developed a thin film of lipid coating. For the whole night, the flask was held in a desiccator under

Table 1 Variable Levels Employed in Box-Behnken Experimental Design

Independent Variables (X)	Coded Value		
	Low (−1)	Medium (0)	High (+1)
Cholesterol (X1) (mg)	20	60	100
Centrifugation Speed (X2) (rpm)	10000	14,000	18000
Sonication time (X3) (min)	10	20	30
Responses (Y)	Constraint		
Particle size (Y1) (nm)	Minimize		
Entrapment efficiency (Y2) (%)	Maximize		
Drug Loading (Y3) (%)	Maximize		

vacuum to make sure that the organic solvent was gone. After that, the lipid film was extensively mixed with water by wetting it using phosphate-buffered solution at pH 7.4 employing a rotary vacuum evaporator and a water bath running at 120 rpm and 65 °C. The dispersion was sonicated for one hour with a bath sonicator (UCB 40, Citizen Industries, Ahmedabad, India), converting multilamellar vesicles (MLVs) into nano-sized unilamellar vesicles (ULVs). The sample was left at ambient temperature for approximately two hours after sonication to encourage vesicle formation before being stored overnight at 4 °C. Then, one hour of centrifugation was done at 15000 rpm. In order to prepare dry powered formulation, the product was gathered, pre-cooled for the night at −20 °C, and then lyophilized for 12 hours in a laboratory lyophilizer (Innova Biomeditech Co., Ltd., Mumbai, India).[29]

Trastuzumab Conjugation to the CBNCs Surface via EDC-NHS Chemistry

Conjugation of TZ over the surface of optimized CBNCs was carried out through a conventional EDC-NHS mechanism as reported elsewhere.[30] The CBNCs that were loaded with TZ were reconstituted in 1 mL of MES buffer at pH-5.5. To activate surface carboxyl (-COOH) groups of CBNCs, they were incubated with 200 µL of EDC (4 mg/mL) and 200 µL (6 mg/mL) for 30 minutes at 25±2 °C on a shaker. Following activation, the CBNCs were cleaned twice with MES buffer (pH 5.5) by centrifugation (15,000 rpm, 15 min, 4 °C) and then suspended again in 1 mL of the same buffer. TZ monoclonal antibody (2.5 mg/mL) was then conjugated to the EDC-NHS-activated CBNCs, followed by 4 hours of incubation at 25±2 °C under continuous shaking to facilitate covalent amide bond formation. For additional examination, the conjugated CBNCs were centrifuged for 45 minutes at 17,500 rpm, then twice washed with PBS (pH 7.4), dispersed again in PBS (pH 7.4), and kept at 2–8 °C until further use. The QPRO-Bicinchoninic Acid (BCA) based protein assay kit (Cyanagen Srl, Italy) was used to determine the trastuzumab conjugation efficiency of the CBNCs, and the calculation was performed using the following formula.[26]

$$\%\,\text{TZ conjugation} = (\text{Amount of TZ added to the CBNC} - \text{Amount of TZ in CBNC supernatant}) \times 100$$

Assessment of Antibody Surface Conjugation on Nanolipid Carrier Using SDS-PAGE Electrophoresis

SDS-PAGE was employed to evaluate antibody conjugation on the surface of CBNCs.[2] Briefly, samples of CBNCs and TZ-CBNCs were resuspended in PBS (20 µL from a 10 mg/mL stock solution). In parallel, free TZ (1 µL) was prepared separately. Each sample was mixed with 5 µL of 2X Laemmli loading buffer and subsequently loaded onto 10% SDS-PAGE gels, accompanied by molecular weight markers. Electrophoresis was performed initially at 80 V for protein stacking, followed by 100 V for protein separation. After electrophoresis, proteins were transferred onto polyvinylidene difluoride membranes at 15 V for 1 h. Membranes were blocked with 5% bovine serum albumin in Tris-buffered saline and incubated overnight at 4°C with HER2-specific secondary antibodies (dilution 1:5000; Cell Signaling Technology or Abcam). Following four consecutive washing cycles (0.1% Tween-20 in buffered saline, 10 min each), protein bands were detected using an enhanced chemiluminescence detection method.

Characterization of Experimental Formulations

Fourier Transform Infrared (FTIR)

FTIR spectroscopy analyzes the interaction among the drug and the excipients in the preparation.[2] Examining pure CB, the excipients utilized, the physical mixing of CB with the excipients, and formulations both with and without the medication were all part of this endeavour. FTIR analysis of TZ and the TZ-conjugated formulation was also performed to verify the incorporation of TZ onto the NCs' surface. All samples were combined with IR-grade potassium bromide (KBr, spectroscopy grade) in a 1:100 proportion, and the pellet was created by compressing them in a hydraulic press under a pressure of ~10 tons for 2–3 minutes. The pellets were analysed using an FTIR analyser (IRAffinity-1, Shimadzu Corporation, Kyoto, Japan). Spectra were recorded in the range of 4000–400 cm^{-1} with a resolution of 4 cm^{-1} and 32 scans per sample. Background correction was performed using a pure KBr pellet. The obtained spectra were compared to identify characteristic peaks of CB, excipients, and TZ, and to evaluate any possible shifts, disappearance, or appearance of new peaks that could indicate drug–excipient interactions or successful antibody conjugation on the surface of NCs.

Differential Scanning Calorimetry (DSC)

Measured amount of pure CB, the excipients, the drug/excipient physical mixture, the formulation, and the blank for DSC analysis was investigated using the differential scanning calorimeter (DSC 204 F1, Netzch, New Castle, Delaware, USA). Over a temperature range of 30 °C to 280 °C, all procedures were conducted in a dynamic nitrogen atmosphere (50 mL/min) with a heating rate of 10 °C per minute. Approximately 3–5 mg of each sample was accurately weighed and sealed in standard aluminum pans with pierced lids. An empty sealed pan was used as a reference. The instrument was calibrated using indium and zinc standards before analysis. Thermograms were recorded and analyzed to identify characteristic endothermic or exothermic transitions. Any shifts or disappearance of peaks were used to evaluate drug–excipient interactions and the incorporation of CB within the formulation.[31]

X-Ray Diffraction (XRD) Analysis

In order to demonstrate the crystallinity or amorphous nature of the laden CB in the formulation, an X-ray diffractometer (Ultima IV, Bruker Corporation, Karlsruhe, Germany) was implemented. We studied the XRD patterns of pure CB, and CBNCs. An anode was operated at a voltage of 40 kV and a current of 15 mA were used by the detector that gathered the scattered radiation data. At a scanning pace of $1° \text{ min}^{-1}$, measurements were taken with a scanning angle ranging from 5° to 70°. Samples (approximately 100 mg) were finely ground, uniformly spread on a glass sample holder, and pressed to obtain a flat surface before measurement. The instrument was calibrated using a standard silicon sample before analysis. Data were collected in continuous scan mode using Cu-Kα radiation (λ = 1.5406 Å), and the obtained diffractograms were analyzed to identify characteristic peaks, changes in intensity, or the disappearance of sharp peaks, indicating conversion from a crystalline to an amorphous state.[32,33]

Percentage of Drug Loading and Entrapment Efficiency

A measured quantity (5 mg) of CBNCs was dissolved in the required amount of ethanol, vortexed, and then centrifuged at 13,500 rpm for 10 minutes. The absorbance of was quantified at 303 nm via a UV/VIS spectrophotometer (UV 3000+, Labindia Instruments Pvt. Ltd., Thane, Maharashtra, India). The concentration of CB was calculated from a previously established calibration curve (2–20 µg/mL, $R^2 > 0.99$). All measurements were performed in triplicate to ensure reproducibility. The proportion of drug loading and drug loading efficiency were determined via the subsequent formula.[34]

$$\text{CB loading}\,(\%) = (\text{amount of CB in CBNCs}/\text{amount of CBNCs obtained}) \times 100$$

$$\text{CB loading efficiency}\,(\%) = (\text{practical CB loading}/\text{theoretical CB loading}) \times 100$$

Particle Size and Zeta Potential

The lyophilized CBNCs/TZ- CBNCs were reconstituted in 2 mL of Milli-Q water, subjected to sonication for 15–20 minutes, and vortexed for several minutes to disaggregate any clumps in the suspension before analysis. Using the Zetasizer Nano ZS 90 (Malvern Instruments, Malvern, UK) with Data Transfer Assistance (DTA) software (Malvern zetasizer Limited, Malvern, UK), samples were analyzed for mean particle size, polydispersity indices (PDI), and zeta potential. Measurements were performed at 25 ± 1 °C in disposable polystyrene cuvettes for particle size/PDI and in folded capillary cells for zeta potential. Each sample was measured in triplicate, and the mean ± standard deviation was reported. Instrument calibration was performed using polystyrene latex bead standards prior to analysis. The hydrodynamic diameter was determined by dynamic light scattering (DLS) at a fixed scattering angle of 90°.[27,34]

Field Emission Scanning Electron Microscopy (FESEM)

The surface morphology of the fabricated CBNCs/TZ-CBNCs was analysed by using an electron microscope (Sigma 500, Zeiss, Germany). Freeze-dried formulations were placed onto carbon tape affixed to a sample stub. A platinum layer was sputter-coated onto the sample for 5 minutes at an accelerating voltage of 10 kV. Imaging was carried out under liquid nitrogen conditions using FESEM. Prior to imaging, the samples were dried under vacuum to remove residual moisture. The sputter-coating thickness was maintained at approximately 10 nm to avoid charging artefacts. Images were captured at multiple magnifications (ranging from 20,000× to 100,000×) to assess particle size, morphology, and surface

characteristics. Representative micrographs were selected for analysis and comparison between non-conjugated and conjugated formulations.[35]

Energy Dispersive X-Ray (EDX) Analysis

EDX, integrated with the scanning electron microscope (Sigma 500, Zeiss, Germany), was utilized to analyze the composition of the CBNCs/TZ-CBNCs. The lyophilized samples were mounted on carbon tape and sputter-coated with a thin platinum layer to enhance conductivity. Spectra were acquired at an accelerating voltage of 15–20 kV under high vacuum conditions. Elemental mapping was performed in addition to point and area scans to confirm the uniform distribution of key elements (C, O, P, N, and others related to lipids, drug, and antibody conjugation). The relative weight % and atomic % of each element were calculated using the instrument's built-in analysis software.

High Resolution Transmission Electron Microscopy (HR-TEM)

HR-TEM was carried out using the CBNCs/TZ-CBNCs to examine the core morphology and distribution profile of the drug. Lyophilized CBNCs/TZ-CBNCs were re-dispersed in Milli-Q water and delicately spread onto a carbon-layered copper grid (300 mesh; Ted Pella Inc., CA, USA), which was subsequently air-dried for 10 hours and imaged using an HR-TEM apparatus (JEM 2100; Thermo Fisher Scientific, Waltham, MA, USA). Samples were stained with 1% (w/v) phosphotungstic acid (PTA, pH 7.0) to enhance contrast, and excess solution was wicked off using filter paper before drying. The instrument was operated at an accelerating voltage of 200 kV. Images were acquired at multiple magnifications to evaluate particle size, shape, and dispersion; representative micrographs were then selected for analysis.[27]

Atomic Force Microscopy (AFM)

AFM (JPK NanoWizard 4, Bruker, Berlin, Germany) analysis was used to study the particle size, surface, and three-dimensional morphology of CBNCs/TZ-CBNCs under typical conditions. The Peak Force QNM (Quantitative Nano Mechanical mapping) mode used a silicon nitride probe with a resonance frequency of 150–350 kHz and a force constant of 0.4 N/m. Lyophilized CBNCs/TZ-CBNCs were reconstituted in Milli-Q water. Following sonication (5 min) and vortexing (5 min), a droplet of the sample was delicately dropped on a precleaned glass slide, which was then subjected to vacuum drying. The designed glass slide was analyzed for AFM imaging. Images were acquired in tapping mode under ambient conditions, with scan sizes ranging from 1 μm × 1 μm to 5 μm × 5 μm at a resolution of 512×512 pixels. Height, phase, and three-dimensional topography images were recorded, and surface roughness parameters (Ra and Rq) were calculated using the instrument's built-in software. Multiple regions of each sample were scanned to ensure reproducibility, and representative images were selected for presentation.[2]

In vitro Drug Release Study

The dialysis bag in phosphate-buffer saline (PBS, pH 7.4) was taken to evaluate the in vitro drug release profile of CBNCs/TZ-CBNCs. A 5 mg sample of freeze-dried preparation was dissolved in 1 mL of PBS (pH 7.4) and transferred into a dialysis bag (Rexon Dialysis Membrane-60, Bangalore, India). Cotton thread tightly bound the two corners of the dialysis bag. As a drug release medium, the full assembly was placed in a 100 mL beaker with 50 mL of PBS (pH 7.4). A magnetic bead was used to stir the device, which was set up on a magnetic stirrer and kept at room temperature at 300 rpm. The molecular weight cut-off (MWCO) of the dialysis membrane was 12–14 kDa, which allowed the free drug to diffuse while retaining nanoparticles. The entire setup was maintained at 37 ± 0.5 °C to mimic physiological conditions. A 1 mL sample was drawn from the drug release medium at designated time points and substituted with an equivalent volume of fresh media. PBS (pH 7.4) was employed as the baseline reference, and the samples were tested at 303 nm through a spectrophotometer. In order to determine the concentration, the calibration curve was used. All experiments were carried out in triplicate, and cumulative drug release (%) was plotted as a function of time.[6,27]

Drug Release Kinetics Study

The experimental NCs' drug release mechanism was investigated by applying different kinetic models to data from in vitro drug release studies. These models included zero-order, first-order, Higuchi, Korsmeyer-Peppas, and Hixson-Crowell, which measured percentage drug remaining against time, cumulative drug release against the square root of

time, and logarithmic cumulative drug release versus logarithmic time, respectively. The calculated R2 values served as a basis for assessing the linearity of the graphs. The model with the highest R^2 value was considered the best fit to describe the release kinetics. The release exponent (n) obtained from the Korsmeyer–Peppas model was used to identify the drug release mechanism (Fickian diffusion, anomalous transport, or case-II transport). All analyses were performed using Microsoft Excel and GraphPad Prism software, and results are expressed as mean ± SD from triplicate experiments.[27]

Stability Studies

The physical stability of the optimized CBNCs was estimated by monitoring the physical appearance, alterations in particle size, zeta potential, and entrapment efficiency over time following ICH guidelines. The formulation (5mL) was stored under refrigerated (4°C ± 2°C, ~30–45% RH), ambient temperature (25°C ± 2°C, 60% RH), and physiological temperature (37°C ± 2°C, 75% RH) conditions. Samples were collected at scheduled periods of 1, 2, and 3 months. Particle size and zeta potential were determined using DLS, while entrapment efficiency was analyzed as previously described. Additionally, TEM was performed post-storage to evaluate vesicle morphology and confirm the absence of aggregation or fusion. All experiments were carried out in triplicate, and results were expressed as mean ± SD.[2]

In vitro Anticancer Effectiveness Analysis

Cytotoxicity Analysis by MTT Assay

Cytotoxicity of CB, CBNCs, and TZ-CBNCs was evaluated on the MCF-7 and SKBR-3 cell lines using MTT (3-(4, 5-dimethylthiazol-2-yl)-2, 5-diphenyl tetrazolium bromide). Briefly, MCF-7 cells and SKBR-3 cells (5,000 per well) were distributed into a 96-well microplate. Next, the CB/CBNCs/TZ-CBNCs with different concentrations (0–50 µg/mL) were applied to the selected wells. Following 24 h incubation at 37 °C in a CO_2 incubator (ESCO, US), 100 µL of MTT (5 mg/mL in PBS; Thermo Fisher Scientific, Waltham, MA, USA) was introduced into every well, and the plates were exposed to 37 °C during incubation for another 4 hours. The addition of dimethyl sulfoxide (100 µL per well) dissolved the intracellular formazan crystals. A microplate reader (SpectraMax, Molecular Devices, USA) was used to measure the color intensity at 540 nm. The half-maximal inhibitory concentration (IC_{50}) values were determined using dose–response curves with non-linear regression analysis in GraphPad Prism software. All experiments were performed in triplicate, and the data are presented as the mean ± SD. The antiproliferative effect of CB/CBNCs/TZ-CBNCs was determined as a percentage of cell growth inhibition, considering concentration and in comparison with the corresponding controls. Cell viability (%) was calculated using the following formula:

$$\text{Cell Viability}\,(\%) = \text{Absorbance of treated cells}/\text{Absorbance of control cells} \times 100$$

Internalization Efficiency Analysis

To assess the internalization efficiency of CBNCs/TZ-CBNCs in the tested MCF-7 and SKBR-3 cells, FITC-labelled formulations were added to 12-well plates seeded with ~1×10^5 cells per well and incubated overnight to allow adherence. The cells were then treated with the formulations at a concentration of 100 ng/mL and incubated for 1 h at 37 °C in a humidified 5% CO_2 incubator. After incubation, the cells were rinsed three times with PBS (pH 7.4) to remove unbound formulations, fixed with 4% paraformaldehyde for 10 min, and counterstained with DAPI (1 µg/mL) to visualize nuclei. Cellular uptake was observed using a fluorescent microscope (Leica Microsystems, Wetzlar, Germany) equipped with a blue filter. Images were acquired using MIA software, and fluorescence intensity was semi-quantitatively analyzed with ImageJ software to compare the degree of internalization between CBNCs and TZ-CBNCs.[26]

Statistical Analysis

To maintain accuracy and reproducibility, all experiments were conducted as three independent repeats where applicable, and the findings were presented as standard deviation (SD) ± mean. Utilizing Origin Pro 8 and GraphPad Prism (version 10.0) software, one-way ANOVA was employed to calculate the statistical data, followed by a Tukey post hoc test. For the experiments, P values ≤ 0.05 at a 95% confidence level were regarded as statistically significant.

Results

A total of 15 runs with three centre points were created using the Box-Behnken design to optimize CBNCs while monitoring three independent and three dependent parameters as shown in Table 2. All generated CBNCs were characterized through investigations of the percentage of drug entrapment, average particle size, and percentage of drug loading. Contour plots were generated to investigate the influence of selected independent variables on the dependent variables.

Impact of Independent Variables on CBNCs Particle Size

It is known that the concentration of cholesterol, the speed of centrifugation, and the time of sonication are not very important in controlling the size of the particles or the release profile of the drug from the matrix. As detailed in Table 2, the particle sizes of CBNC formulations ranged from 192.9 nm to 197.32 nm due to various combinations of variables. This variation in size was analysed using the derived quadratic model equation.[28]

$$Particle\,Size\,(nm)(Y1) = 195.04 - 0.2500X1 - 0.3750X2 - 0.5000X3$$
$$- 0.2500X1X2 - 0.2500X1X3 + 0.2500X2X3 + 0.2300X1^2 - 0.2700X2^2 - 0.0200X3^2$$

The polynomial equation indicated that a positive value denoted a synergistic effect, while a negative value indicated an antagonistic effect. The model was validated as significant (F-value = 0.1488; $P < 0.05$), confirming its relevance in guiding the experimental design.

The polynomial equation revealed that an increase in cholesterol concentration (X1) resulted in a decrease in CBNCs particle size. An elevation in the concentration of X1 resulted in a decrease in the particle size of CBNCs due to membrane

Table 2 Experimental Design Using Box-Behnken and Corresponding Observed Responses

Formulation Code	Cholesterol (X1)	Centrifugation Speed (X2)	Sonication Time (X3)	Particle Size (nm)	Entrapment Efficiency%	Drug Loading%
CBNC1	20	14,000	30	195.19	79	8.2
CBNC2	100	18,000	20	195.5	78.6	8
CBNC3	60	14,000	20	195.4	78.23	8.5
CBNC4	60	10,000	30	196.23	79.02	8.6
CBNC5	100	10,000	20	194.9	78.99	8.7
CBNC6	60	10,000	10	197.32	78.56	8.4
CBNC7	60	14,000	20	196.15	79.32	8.3
CBNC8	60	14,000	20	194.3	79.66	8.4
CBNC9	60	14,000	20	192.9	79.54	8.45
CBNC10	60	18,000	10	193.5	78.22	8.65
CBNC11	20	10,000	20	194.24	79.65	8.7
CBNC12	20	14,000	10	196.64	80.22	8.2
CBNC13	60	18,000	30	193.58	81.22	8.4
CBNC14	100	14,000	10	196.8	82.13	8.7
CBNC15	20	18,000	20	196.5	83.01	8.6
CBNC16	100	14,000	30	194.4	81.87	8.22
CBNC17	60	14,000	20	197.2	81.64	8.31

https://doi.org/10.2147/IJN.S541332

stabilization, but excessive cholesterol gave rise to a slight rising in particle size. Increasing the centrifugation speed also reduced particle size by getting rid of larger vesicles. However, the sonication time had the most significant effect, as longer exposure made the vesicles smaller. Interaction effects indicated that elevated levels of X1 and X3 further diminished size, although high levels of X2 and X3 might marginally enhance size due to vesicle restructuring.[36] These results underscored the need to optimize parameters for the production of monodisperse, stable CBNCs, as illustrated in Figure 1A–C

Impact of Independent Variables on CBNCs % Entrapment Efficiency

In the formulated CBNCs, drug entrapment range was observed to range between 78.22% and 83.01%. The model presented the below polynomial equation to characterize the influence of the independent variables on the percentage entrapment efficiency:

$$EE\%\,(Y2) = 79.68 - 0.0362X1 + 0.6038X2 + 0.2475X3 - 0.9375X1X2 + 0.2400X1 + 0.6350X2X3 + 0.9672X1^2 - 0.5828X2^2 - 0.1598X3^2$$

The proportion of drug entrapment is positively impacted when a positive value comes before a factor, and negatively impacted when a negative value comes before a factor. Statistical significance was found for this model (F-value = 0.5100;

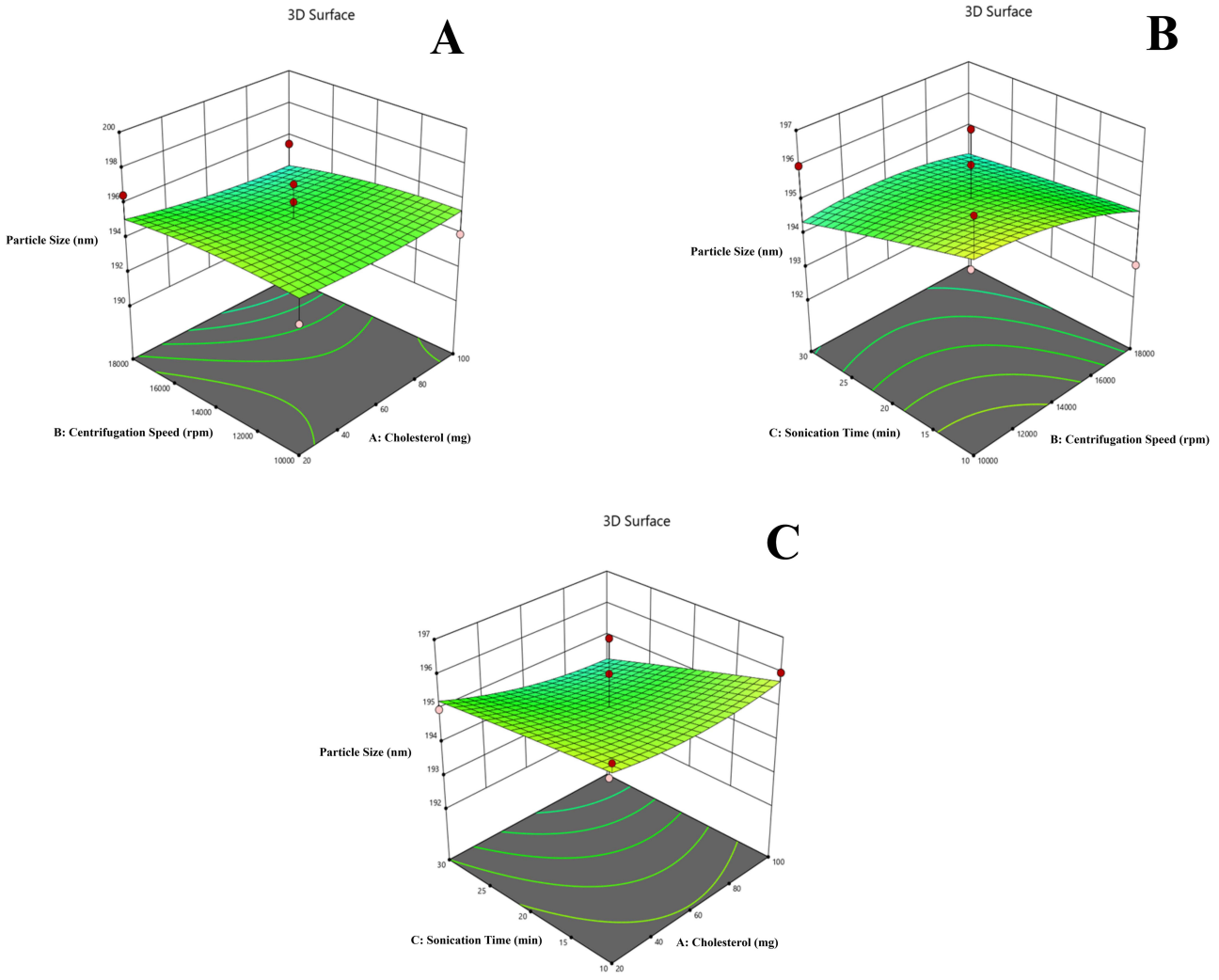

Figure 1 (**A**) A response surface plot displaying how the amount of cholesterol and the speed of the centrifugation affect the particle size when the sonication time stays the same. (**B**) A response surface plot that shows how the speed of the centrifugation and the time of the sonication affect the particle size when the cholesterol concentration stays the same. (**C**) A response surface plot presenting how the amount of cholesterol and the time of sonication change the particle size when the centrifugation speed remains constant.

P < 0.05). The examination of the polynomial equation revealed that when factor X1 (cholesterol concentration) values decreased, the percentage of drug entrapment rose.[37] Additionally, factor X2 (centrifugation speed) exhibited a positive effect on the entrapment efficiency. However, factor X3 had major impact on the drug entrapment efficiency, as depicted in Figure 2A–C.

Impact of Independent Variables on CBNCs % Drug Loading

The variations in % drug loading are described by the quadratic equation below:

$$DL\%(Y3) = 8.39 - 0.0100X1 - 0.0937X2 - 0.0662X3 - 0.1500X1X2 - 0.1200X1X3 - 0.1125X2X3 - 0.0373X1^2 + 0.1452X2^2 - 0.0247X3^2$$

The model demonstrated statistically significant (F-value = 1.03; $P< 0.05$). Concentration of cholesterol exhibited antagonistic effect on drug loading while centrifugation time and sonication time had no notable impact, as shown in Figure 3A–C.

Optimization

The optimized CBNCs was chosen by putting constraints on the dependent variables, as illustrated in Table 1. The point prediction from Design Expert software version 13 was employed to predict the optimized CBNCs, focusing on

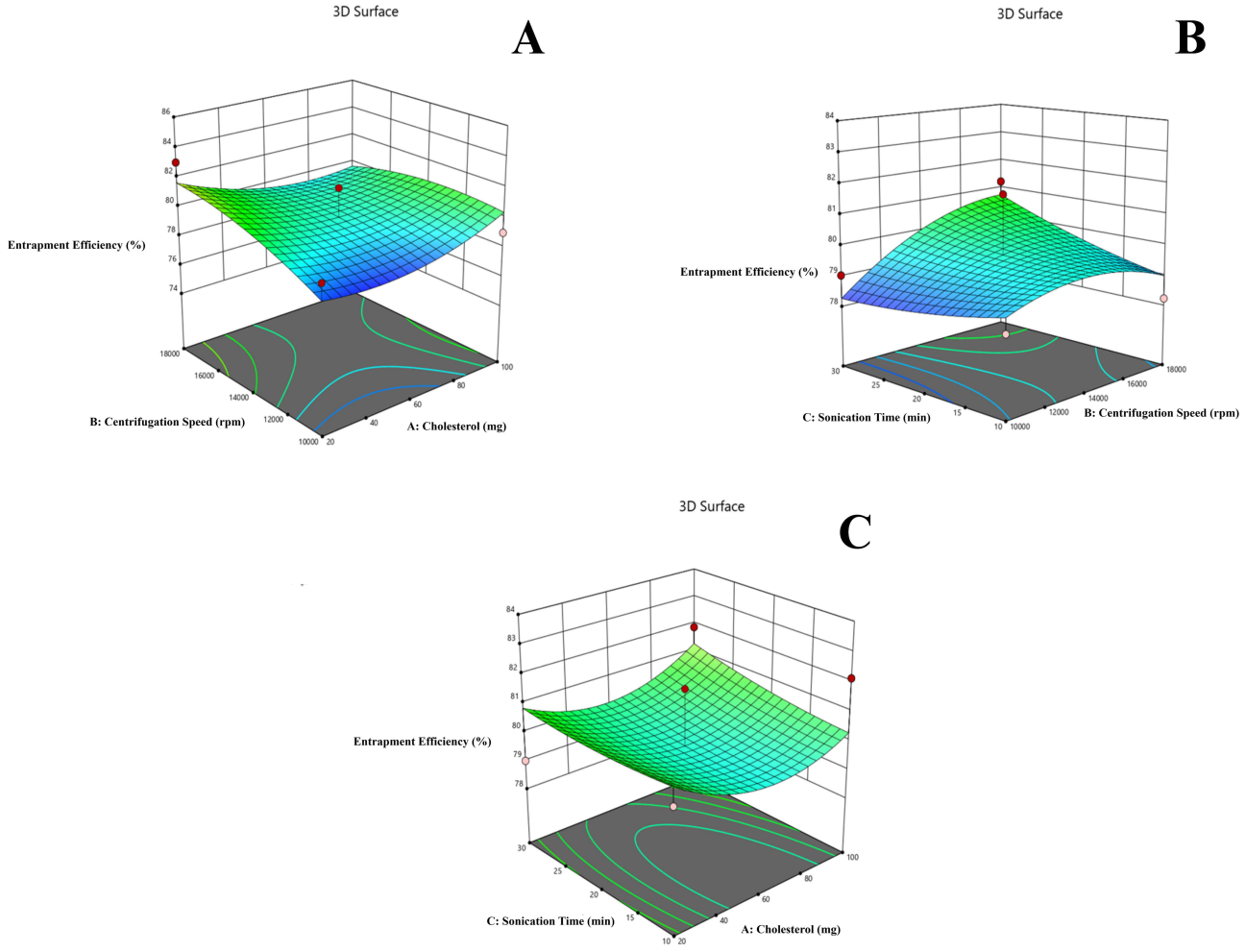

Figure 2 (**A**) A response surface plot illustrating the correlation between the cholesterol concentration and centrifugation speed on the entrapment efficiency, keeping at sonication time constant. (**B**) A response surface plot depicting how the speed of the centrifugation and the time of the sonication affect the efficiency of entrapment when the concentration of cholesterol stays the same. (**C**) A response surface plot presenting how the amount of cholesterol and the sonication time affect the efficiency of entrapment when the centrifugation speed remains constant.

https://doi.org/10.2147/IJN.S541332

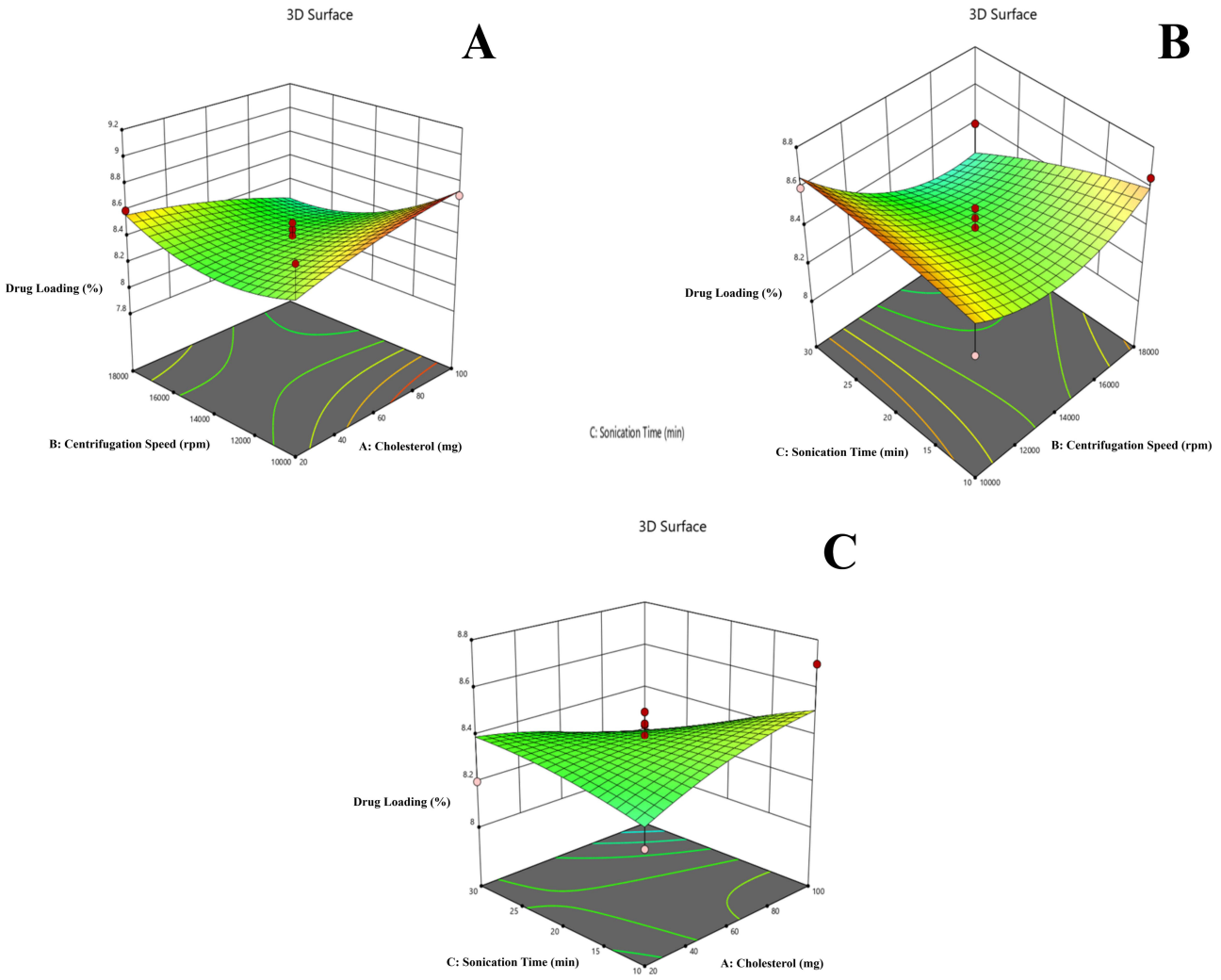

Figure 3 (**A**) A response surface plot showing how the amount of cholesterol and the speed of the centrifugation affect the drug loading when the sonication time stays the same. (**B**) A response surface plot that shows how the speed of the centrifugation and the time of the sonication affect the drug loading when the cholesterol concentration stays the same. (**C**) A response surface plot demonstrating the interaction between the cholesterol concentration and sonication time affecting the drug loading at a constant cholesterol concentration.

achieving a desirability factor approaching 1. This study predicted that the best process parameters would be cholesterol concentration (*X*1) at 60 mg, centrifugation speed (*X*2) at 14,000 rpm, and sonication duration (*X*3) at 20 minutes. It was also predicted that the response values as particle size (Y1): 195.04 nm, entrapment efficiency (Y2): 79.67% and drug loading (Y3) 8.39%.

The selected optimized parameters were taken to produce CBNCs, which showed comparative linearity in between predicted and actual values. The experimental values for the selected parameters were: particle size (Y1) as 194.6 nm, entrapment efficiency (Y2) as 79.8%, and drug loading (Y3) as 8.5%. Overall, the experimental values of the optimized formulation were very adjacent to the predicted values, and thus rationalized the use of the RSM model.[28,37]

TZ Conjugation Efficiency on CBNCs

The conjugation efficiency of TZ onto CBNCs was determined using a BCA protein assay by measuring the unbound antibody in the supernatant after the conjugation reaction. The calculated conjugation efficiency was approximately $67.3 \pm 1.5\%$, indicating successful surface functionalization of TZ over CBNCs.

SDS-PAGE Electrophoresis

In the gel electrophoresis (Figure 4), the band for the TZ and the TZ-CBNCs was observed in the same line, indicating that the antibody successfully conjugated to the CBNCs surface while retaining its characteristic migration pattern.

Fourier Transform Infrared (FTIR) Spectroscopy

The FTIR study of CB revealed different functional groups in its various excipients, their physical mixtures, and both non-conjugated and antibody-conjugated formulations. Data depicted the successful conjugation of TZ over CBNCs. Pure capecitabine had characteristic peaks on a stretching vibration of C=O observed near 1700 cm^{-1} and N-H bending at approximately 1600 cm^{-1}, which are its main functional groups. The excipients, such as SL, CHT, and BHT, showed important bands in the phosphate groups (1000–1200 cm^{-1}) and the C-H stretching area (2800–3000 cm^{-1}). The FTIR spectrum of the physical mixture, which had CB and other ingredients, showed peaks that were typical of each of the parts. There were no new, significant peaks, suggesting the absence of undesirable chemical interactions. The CBNCs showed a slight shift and lessening of the intensity of CB's main peaks, which means that the drug was effectively encapsulated by the lipid matrix and potential interactions between CB and lipid constituents. The TZ- CBNCs had further adjustments in the spectrum, especially bands near 1650 cm^{-1} and 1550 cm^{-1}, corresponding to amide I and II, respectively, which confirms the successful conjugation of TZ via hydrogen bonding or electrostatic interactions. Moreover, the (-OH) stretching area (~3200–3400 cm^{-1}) exhibited broadening, suggesting hydrogen bonding interactions between TZ and lipid constituents, which may contribute to the stability of the conjugated formulation. The absence of new peaks in both formulations indicated the absence of any undesirable chemical interactions, whereas the observed spectrum shifts indicated a steady incorporation of CB and TZ in the liposomal matrix. FTIR spectra of pure drug, specific constituents, physical mixture, Blank NCs, CBNCs and TZ-CBNCs as shown in Figure 5.

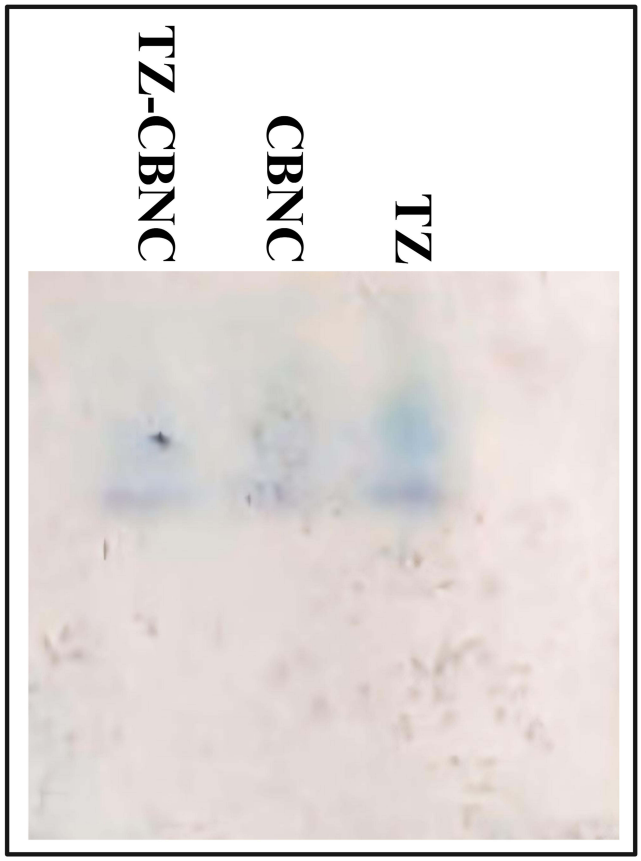

Figure 4 SDS-PAGE gel electrophoresis of trastuzumab (TZ), capecitabine-loaded nanolipid carriers (CBNCs), and trastuzumab-conjugated capecitabine-loaded nanolipid carriers (TZ-CBNCs).

https://doi.org/10.2147/IJN.S541332

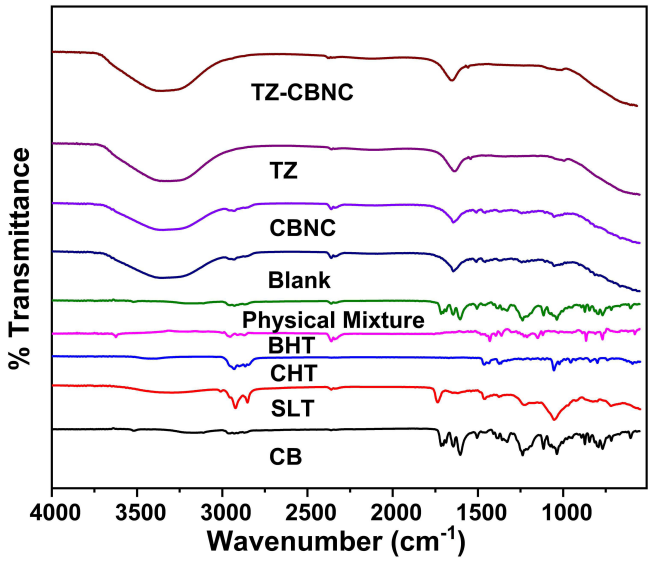

Figure 5 FTIR spectra of pure drug, specific constituents, physical mixture, blank nanolipid carriers (NCs), capecitabine-loaded nanolipid carriers (CBNCs), and trastuzumab-conjugated capecitabine-loaded nanolipid carriers (TZ-CBNCs).

Differential Scanning Calorimetry (DSC)

Different thermal changes were seen in the DSC study of CB, excipients, the physical mixture, blank CBNCs (without drug), and CBNCs. The DSC thermogram of CB displayed a sharp endothermic peak at 160°C, suggesting its crystalline characteristics. SL and CHT exhibited distinct thermal transitions at approximately 240.39°C and 148.23°C, respectively, which correspond to their melting temperature. The physical mixture exhibited thermal events with peaks at around 158°C, 238°C, and 147°C, indicating no substantial chemical reactions. CBNCs exhibited a melting point of 152.3°C as shown in Figure 6, confirming the molecular dispersion of the drug within the lipid bilayer. The broad and attenuated nature of this transition, along with the absence of a sharp CB peak, indicates reduced crystallinity of CB. The absence of a distinct melting peak for CB in the optimized CBNCs indicated its conversion from a crystalline to an amorphous form, suggesting improvements in the drug's solubility, faster dissolution, and enhanced bioavailability..

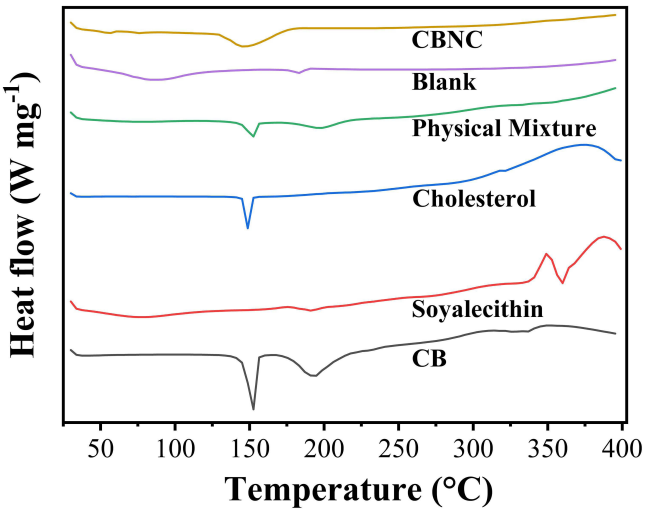

Figure 6 DSC of pure drug, individual components, physical mixture, blank nanolipid carriers (NCs), and capecitabine-loaded nanolipid carriers (CBNCs).

X-Ray Diffraction (XRD)

The XRD analysis of CB and optimized CBNCs revealed a significant reduction in crystallinity upon encapsulation. The pure CB displayed sharp, intense characteristic peaks at 2θ values of 9.6°, 13.4°, 16.9°, 18.4°, 22.5°, and 27.6° confirming its high crystalline nature as shown in Figure 7. In contrast, the formulated CBNCs exhibited a broad and diffused pattern, with a disappearance in the intensity of these characteristic peaks. This change demonstrated the successful addition of CB to the lipid bilayer, transforming it into an amorphous state. The amorphization of CB is expected to improve its solubility and dissolution profile, potentially enhancing drug release and bioavailability from the nanocarrier system.

Average Particle Size and Zeta Potential

The CBNCs had an average particle size of 194.6 nm and a PDI of 0.2501, which means they were stable and could be used for passive tumor targeting. Optimized CBNCs had a zeta potential of −25.55 mV, as shown in Figure 8A, which means they were stable in a colloidal form because the particles would repel each other electrostatically. After conjugation with TZ, the particle size increased to 262 nm, followed by a rise in PDI to 0.6832, indicating an effective TZ conjugation and a little reduction in size uniformity due to steric effects. The zeta potential markedly increased to −57.76 mV (Figure 8B), indicating enhanced surface charge and improved electrostatic stabilization. The increase in zeta potential also implies a higher repulsion between particles, which is likely to prevent aggregation and improve stability during storage and in biological fluids. Furthermore, the larger particle size and increased surface charge after TZ conjugation may influence cellular uptake and receptor-mediated targeting efficiency.

Field Emission Scanning Electron Microscopy (FESEM)

FESEM images of CBNCs and TZ-CBNCs were analyzed and illustrated in Figure 9A and B. Unconjugated formulation (ie, optimized CBNCs) was uniformly round and had an average particle size of 16–23 nm. On the other hand, the TZ-CBNCs had a slightly larger size, averaging around 24–55 nm. The surface exhibited a lower smoothness, with a rough texture relative to the non-conjugated formulation. The structural heterogeneity across the formulations depicted

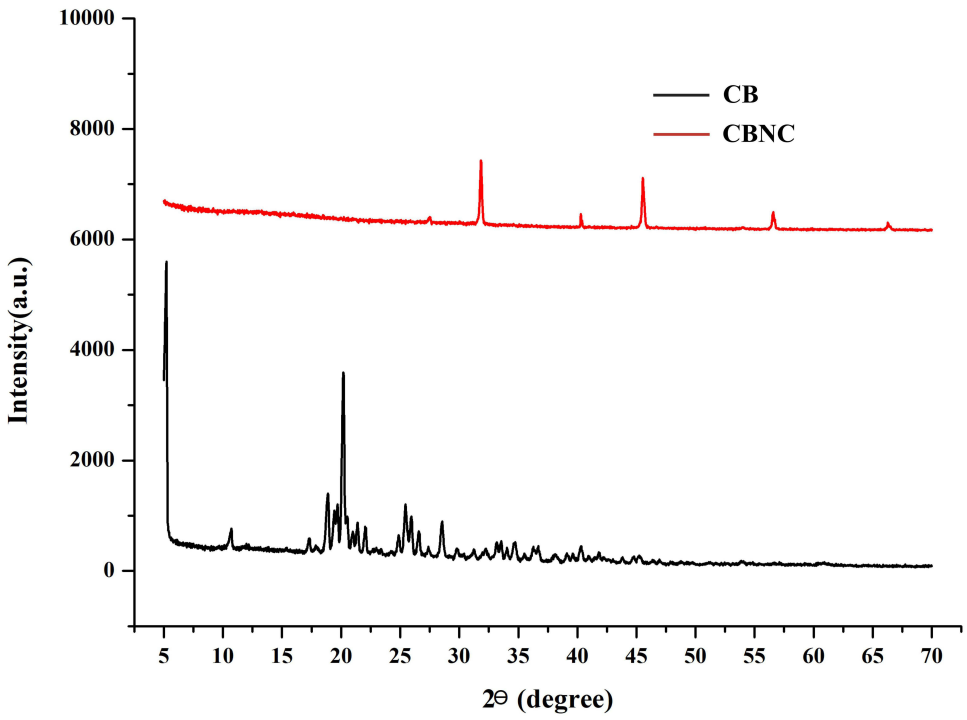

Figure 7 XRD of pure dug and capecitabine-loaded nanolipid carriers (CBNCs).

https://doi.org/10.2147/IJN.S541332

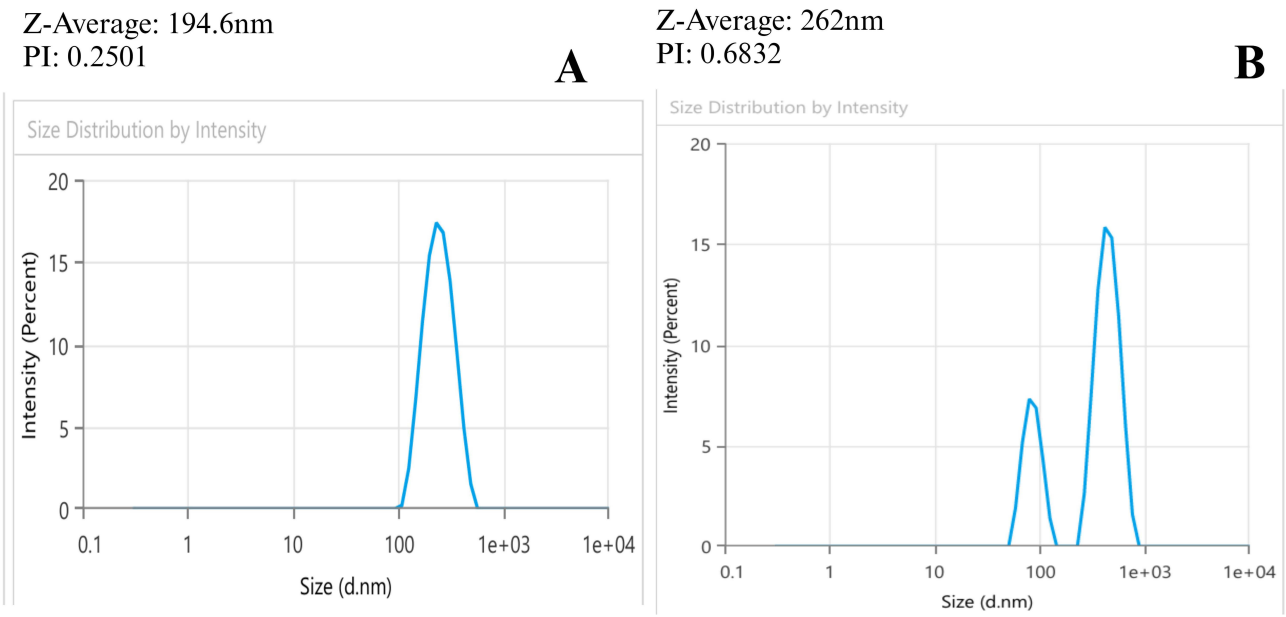

Figure 8 Particle size of experimental nanolipid carriers (NCs). (**A**) Capecitabine-loaded nanolipid carriers (CBNCs) and (**B**) trastuzumab-conjugated capecitabine-loaded nanolipid carriers (TZ-CBNCs).

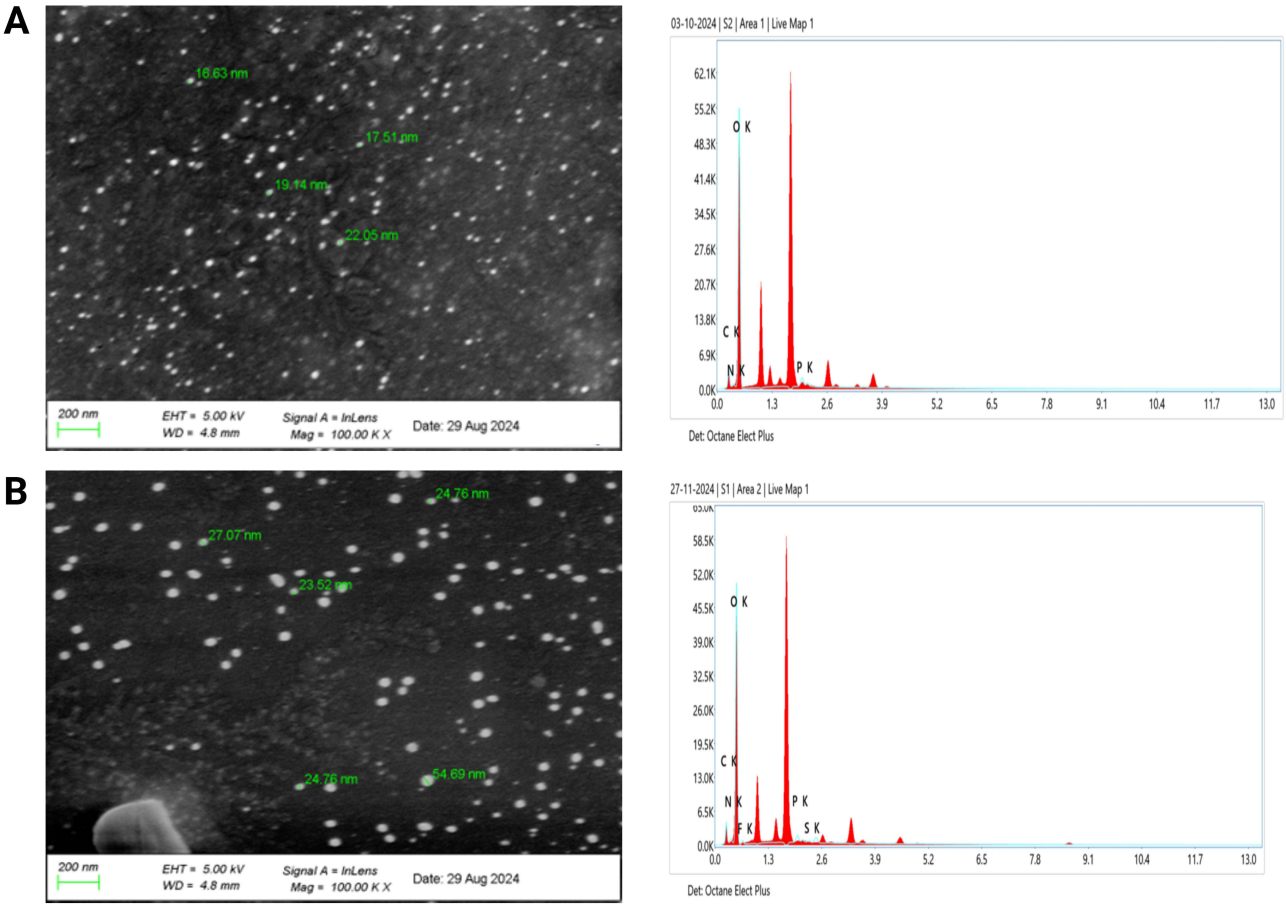

Figure 9 FESEM and EDX images of experimental nanolipid carriers (NCs). (**A**) Capecitabine-loaded nanolipid carriers (CBNCs) and (**B**) trastuzumab-conjugated capecitabine-loaded nanolipid carriers (TZ-CBNCs).

conjugation of TZ. Further, no lumps or large agglomerates were observed throughout the sample maintained colloidal stability post-conjugation.

Energy Dispersive X-Ray (EDX) Analysis

Elemental composition of both CBNCs and TZ-CBNCs was accessed using EDX analysis. The primary elements detected in CBNCs included carbon (C), oxygen (O), nitrogen (N), and phosphorus (P). This evidence indicates the presence of core excipients and drug components. In contrast, the TZ-CBNCs demonstrated an additional presence of sulfur (S) along with a significant increase in nitrogen content, confirming the successful conjugation of the targeting moiety. Since sulfur was not a component in the CBNCs, it was likely that the functionalization process successfully added TZ over CBNCs. Also, the small differences in the amounts of oxygen and phosphorus in the two samples showed that the conjugate and the excipient matrix might interact with each other. These results overall confirmed the successful conjugation process while preserving the structural integrity of the formulations. The energy-dispersive X-ray analysis of the prepared formulations CBNCs and TZ-CBNCs is shown in Table 3.

High Resolution Transmission Electron Microscopy (HR-TEM)

The morphological study exhibited a smooth surface with no aggregation. The HR-TEM images exhibited a globular morphology exhibiting a clear core-shell appearance. Altering TZ on the CBNCs surface might lead to a minor enhancement in the structure, as shown by the HR-TEM images. However, the formulations showed intact vesicles and a unilamellar nature. No distortion in the outer lipid bilayer or internal morphology was observed, suggesting successful formulation. The HR-TEM images of CBNCs and TZ-CBNCs are shown in Figure 10A and C.

Atomic Force Microscopy (AFM)

AFM analysis showed a difference in surface texture among CBNCs and TZ-CBNCs. The image depicted a smooth, uniform topography of CBNCs with an average surface height of approximately 15.5 nm (Figure 11A). However, TZ-CBNCs (Figure 11B) depicted nano-sized clusters that were 37.7 nm in height and had an amplitude value of 19.5 mV. These observations indicated an increase in surface heterogeneity upon TZ conjugation. Furthermore, tiny particles were shown to group to form clusters, which further supported the surface alteration. The surface of the TZ-CBNCs was relatively rougher than that of their non-conjugated counterparts, which might be due to TZ conjugation.

In vitro Drug Release and Analysis of Release

The in vitro cumulative drug release graph illustrated the release profiles of CB, CBNCs and TZ-CBNCs over 72 h. CB at its free form released at the fastest rate (97.45%) within 8 h, indicating burst release tendency. Contrary to that, CBNCs exhibited a biphasic-release pattern, with an initial burst release of ~40% within 8 h followed by a prolonged and controlled release phase, reaching ~92.25% at 72 h. This controlled release pattern reflects efficient encapsulation and diffusion-mediated release from the nanocarrier matrix. TZ-CBNCs demonstrated the slowest drug release among the tested formulations, achieving approximately 84.26% after completion of 72 h as shown in Figure 12. This trend overall suggested that TZ conjugation further restricts drug diffusion across the lipid bilayer and enhances sustained release properties.

Various mathematical models—Zero Order, First Order, Higuchi, Korsmeyer-Peppas, and Hixson-Crowell, etc., were used to predict the mechanism of CB release from CBNCs/TZ-CBNCs. From the coefficient of regression (R^2) values, the best-fit model was predicted (Table 4). The CB had the highest R^2 value for the Zero-Order model (0.995), followed

Table 3 Energy Dispersive X-Ray (EDX) Analysis

Formulations	CK		NK		OK		FK		PK		SK	
	Weight%	Atomic%	Weight%	Atomic%	Weight%	Atomic%	Weight%	Atomic%	Weight%	Atomic%	Weight%	Atomic%
CNL	18.7	23.5	1.8	1.9	78.3	73.9	–	–	1.3	0.6	–	–
TZ-CNL	19.7	24.8	2.2	2.4	74.3	70.1	2.7	2.1	0.9	0.5	0.2	0.1

https://doi.org/10.2147/IJN.S541332

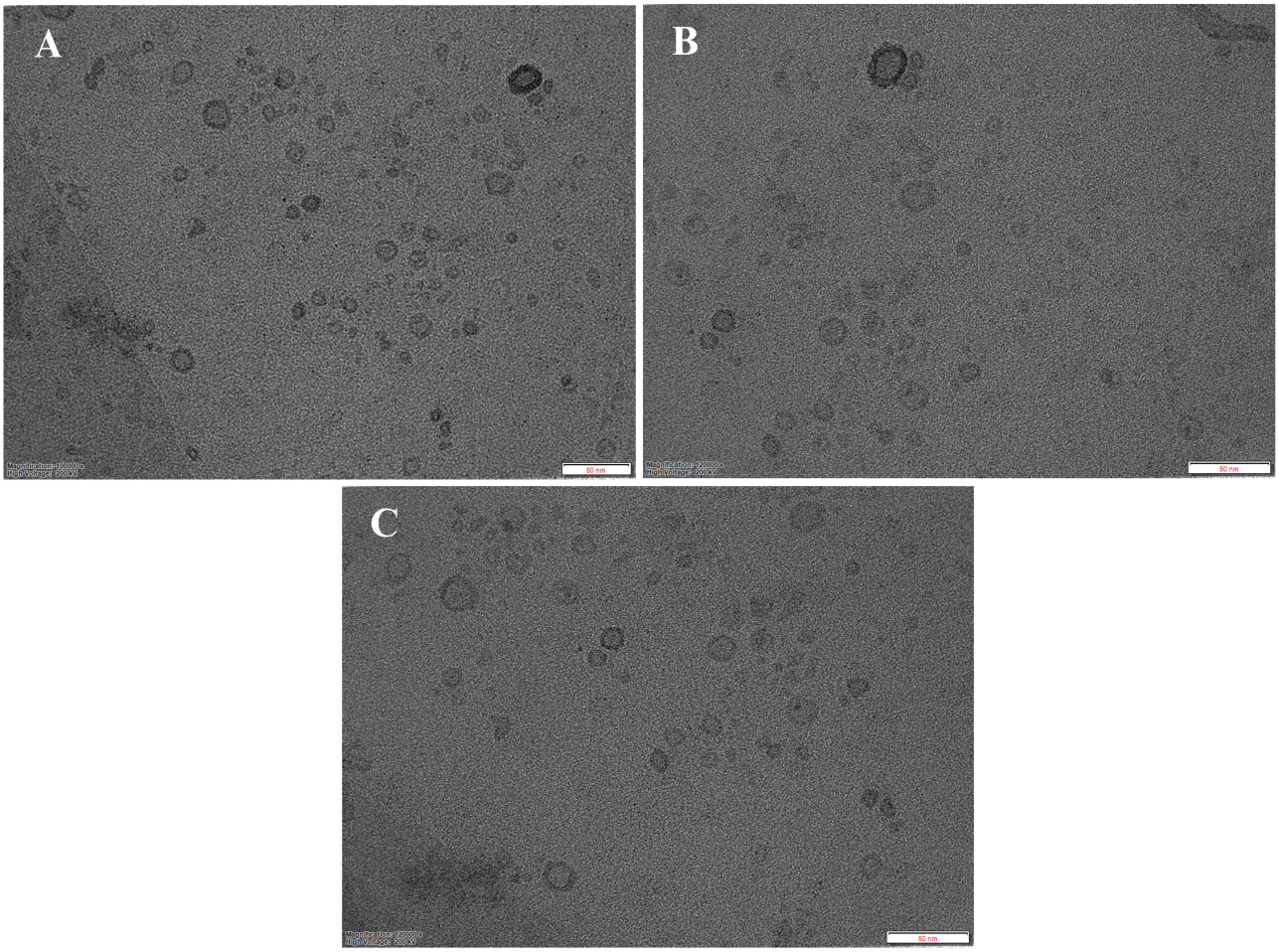

Figure 10 TEM images of optimized nanolipid carriers. (**A**) Capecitabine-loaded nanolipid carriers (CBNCs) (freshly prepared), (**B**) capecitabine-loaded nanolipid carriers (after 3 months under recommended storage conditions), and (**C**) trastuzumab-conjugated capecitabine-loaded nanolipid carriers (TZ-CBNCs).

by Korsmeyer-Peppas (0.986) and Higuchi (0.989). The First Order and Hixson-Crowell models, on the other hand, had significantly lower fits with R^2 values of 0.905 and 0.610, respectively. While Hixson-Crowell again exhibited a poor match (0.458), the CBNCs similarly followed First Order kinetics most strongly (0.981), with excellent correlation in Korsmeyer-Peppas (0.969) and Higuchi (0.962) models. Likewise, the TZ-CBNCs showed a predominant first-order release profile (0.953), along with good fits to Higuchi (0.950) and Korsmeyer-Peppas (0.937) models, but somewhat lower correlation with zero-order and Hixson-Crowell models (Figure 13).

Stability Study

The physical appearance of CBNCs at one, two, and three-month intervals, at 4°C ± 2°C, 24°C ± 2°C, 60% RH, and 37°C ± 2°C, 75% RH was assessed. Except at 37°C, the optimized 0CBNCs kept at 4°C and 24°C were shown to be stable monitoring particle size, zeta potential, and entrapment efficiency over three months under various storage conditions 4°C, 25°C, and 37°C, allowed one to assess the stability of CBNCs. At 4°C, negligible changes were seen, with particle size rising from 194.6 nm to 205 nm and zeta potential marginally dropping from 79.8% to 78.57%. Ranging from −25.55 mV to −24.78 mV, zeta potential values stayed fairly constant, suggesting high colloidal stability. Over three months at 24°C, particle size rose to 207.4 nm, entrapment efficiency fell to 76.23%, and zeta potential fell marginally to −23.67 mV. At 37°C, where particle size rose to 217.8 nm, entrapment efficiency fell significantly to 73.72%, and zeta potential dropped to −22.90 mV (Table 5); the most notable alterations took place, indicating reduced electrostatic repulsion and a tendency toward particle aggregation and lower stability under higher temperature

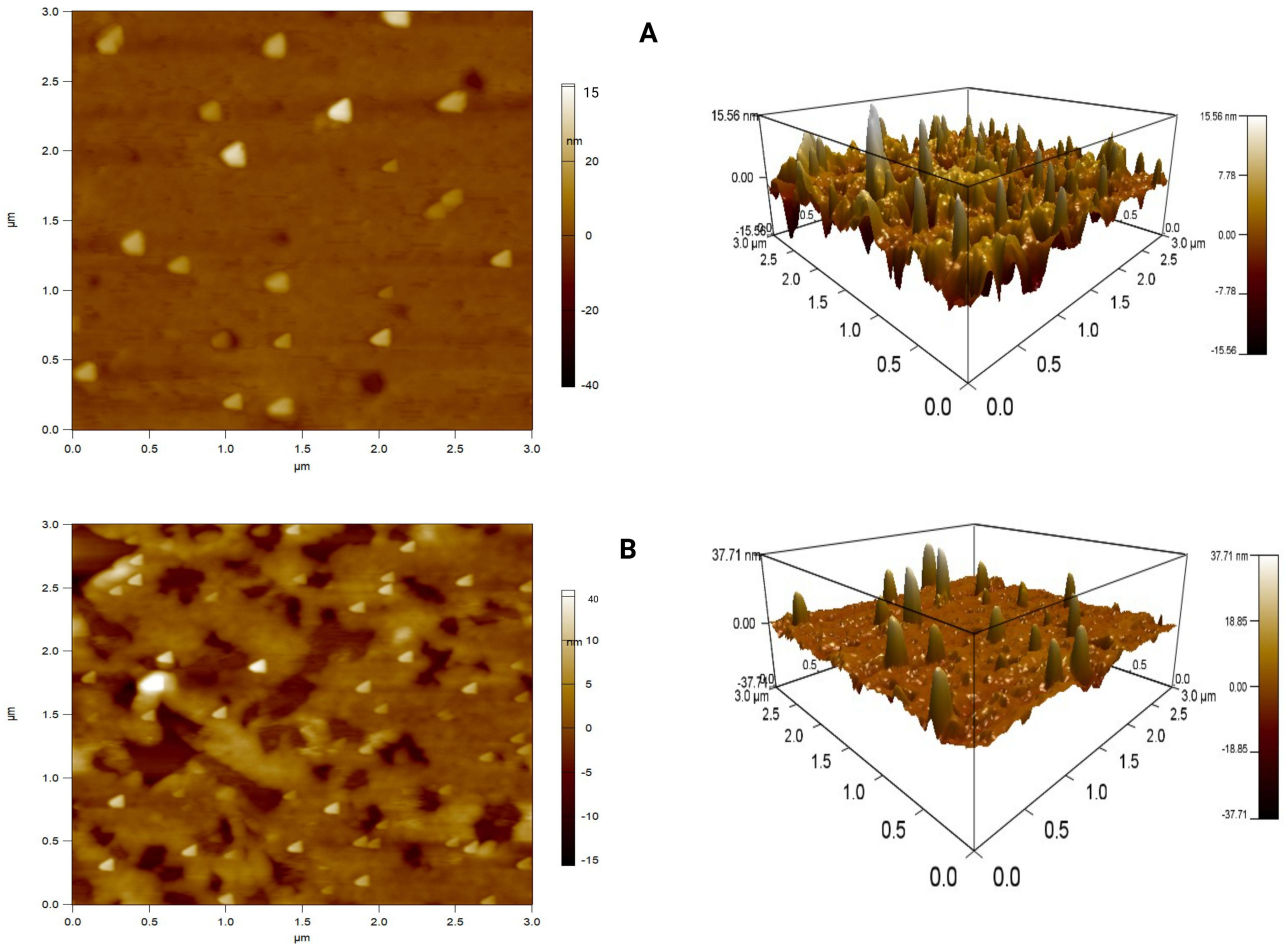

Figure 11 AFM images of experimental nanolipid carriers (NCs). (**A**) Capecitabine-loaded nanolipid carriers (CBNCs), and (**B**) trastuzumab-conjugated capecitabine-loaded nanolipid carriers (TZ-CBNCs).

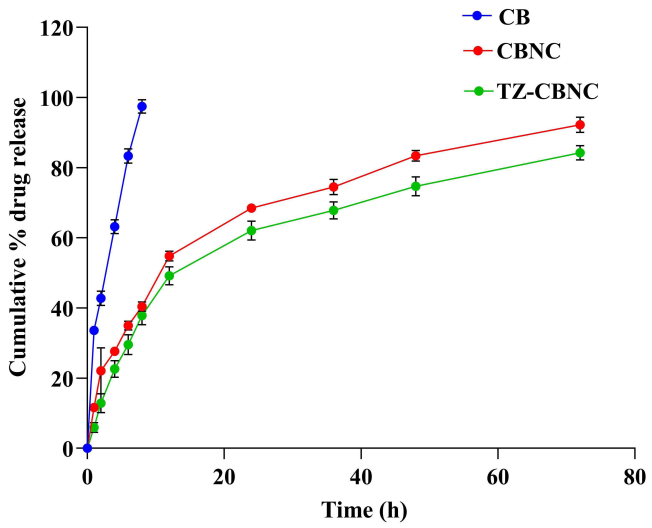

Figure 12 In vitro drug release profile of free capecitabine (CB), capecitabine-loaded nanolipid carriers (CBNCs), and trastuzumab conjugate trastuzumab-loaded nanolipid carriers (TZ-CBNCs). Data represented as mean ± SD (n=3).

https://doi.org/10.2147/IJN.S541332

Table 4 In vitro Drug Release Kinetics (R2, K and n Values) and Mechanism of Drug Release

Formulation Code	Zero Order		First Order		Higuchi		Hixon Crowell		Korsmeyer Peppas		n	Release Mechanism	Release Kinetics
	R^2	K	R^2	K	R^2	K	R^2	K	R^2	K			
CB	0.995	9.336	0.905	−0.413	0.989	35.841	0.610	0.427	0.986	0.529	0.529	Non-Fickian	Zero order
CBNC	0.846	1.073	0.981	−0.033	0.962	10.791	0.458	0.037	0.969	0.466	0.466	Non-Fickian	First order
TZ-CBNC	0.823	1.033	0.953	−0.025	0.95	10.468	0.492	0.038	0.937	0.588	0.588	Non-Fickian	First order

circumstances. HR-TEM analysis further corroborated these findings, showing that CBNCs kept at 37 °C exhibited partial vesicle deformation, irregular morphology, and early signs of aggregation (Figure 10B).

MTT Assay

The MTT assay demonstrated a concentration-dependent reduction in cell viability, with trastuzumab-functionalized nanocarriers exhibiting superior cytotoxic activity compared to unconjugated CBNCs and free CB. The dose–response curves displayed a characteristic sigmoidal pattern, supporting the concentration-dependent nature of the cytotoxic response (Figure 14A and B). In MCF-7 cells, the calculated IC50 values were 37.11 ± 4.8 µg/mL for free CB, 24.05 ± 3.2 µg/mL for CBNCs, and 13.21 ± 2.7 µg/mL for TZ-CBNCs. In contrast, SKBR3 cells, which overexpress HER2 receptors, exhibited lower IC50 values of 26.81 ± 4.5 µg/mL for free CB, 13.33 ± 3.4 µg/mL for CBNCs, and 8.21 ± 1.6 µg/mL for TZ-CBNCs. The consistently reduced IC50 values of TZ-CBNCs across both cell lines, with the most pronounced effect in SKBR3, highlight the enhanced cytotoxic potential conferred by TZ functionalization. Statistical evaluation confirmed that the differences between TZ-CBNCs and other treatment groups were significant ($p < 0.05$, indicated by). The overall cytotoxicity followed the order CB < CBNCs < TZ-CBNCs, with a more substantial therapeutic advantage in HER2-overexpressing SKBR3 cells, thereby corroborating the HER2-targeted efficacy of the developed TZ-CBNCs.

Fluorescent Microscopic Analysis of Cellular Uptake

Fluorescence microscopy was used to evaluate the cellular uptake of FITC-labeled formulations in MCF-7 and SKBR3 cells following a 1-hour exposure to 100 ng/mL of FITC-CBNCs or FITC-TZ-CBNCs (Figure 15A–C). Minimal fluorescence was observed in the FITC-only group, confirming negligible nonspecific uptake. In contrast, both FITC-CBNCs and FITC-TZ-CBNCs exhibited appreciable intracellular fluorescence, indicating effective nanocarrier internalization. Notably, cells treated with FITC-TZ-CBNCs exhibited significantly higher fluorescence intensity compared to those treated with FITC-CBNCs in both MCF-7 and SKBR3 cells (Figure 15D and E), as confirmed by quantitative analysis ($p < 0.05$). This enhancement can be attributed to trastuzumab-mediated recognition and interaction with HER2 receptors, thereby facilitating receptor-mediated endocytosis. The higher fluorescence intensity in SKBR3 cells, which overexpress HER2, further substantiates the targeting advantage of TZ-functionalization. Collectively, these findings confirm that TZ-CBNCs achieve superior intracellular accumulation relative to unconjugated CBNCs, validating the potential of the system to exploit both passive (EPR effect) and active (HER2-targeted) uptake mechanisms for effective breast cancer therapy.

Discussion

CB is an orally administered prodrug of 5-fluorouracil (5-FU) and is commonly prescribed for treating cancers like breast, colorectal, and gastric. CB undergoes enzymatic to 5-FU in tumor environments, where it inhibits thymidylate synthase, interferes DNA synthesis and triggers cell death in rapidly dividing cancerous cells. Its tumor-selective activation enhances therapeutic efficacy while minimizing systemic toxicity.[38] Elevated HER2 expression is associated with cellular change and metastasis in high-grade breast tumors.[39,40] The main therapy for HER2-positive breast malignancy is TZ. Numerous strategies are employed to target HER2-positive breast cancer cells, including as antibody-

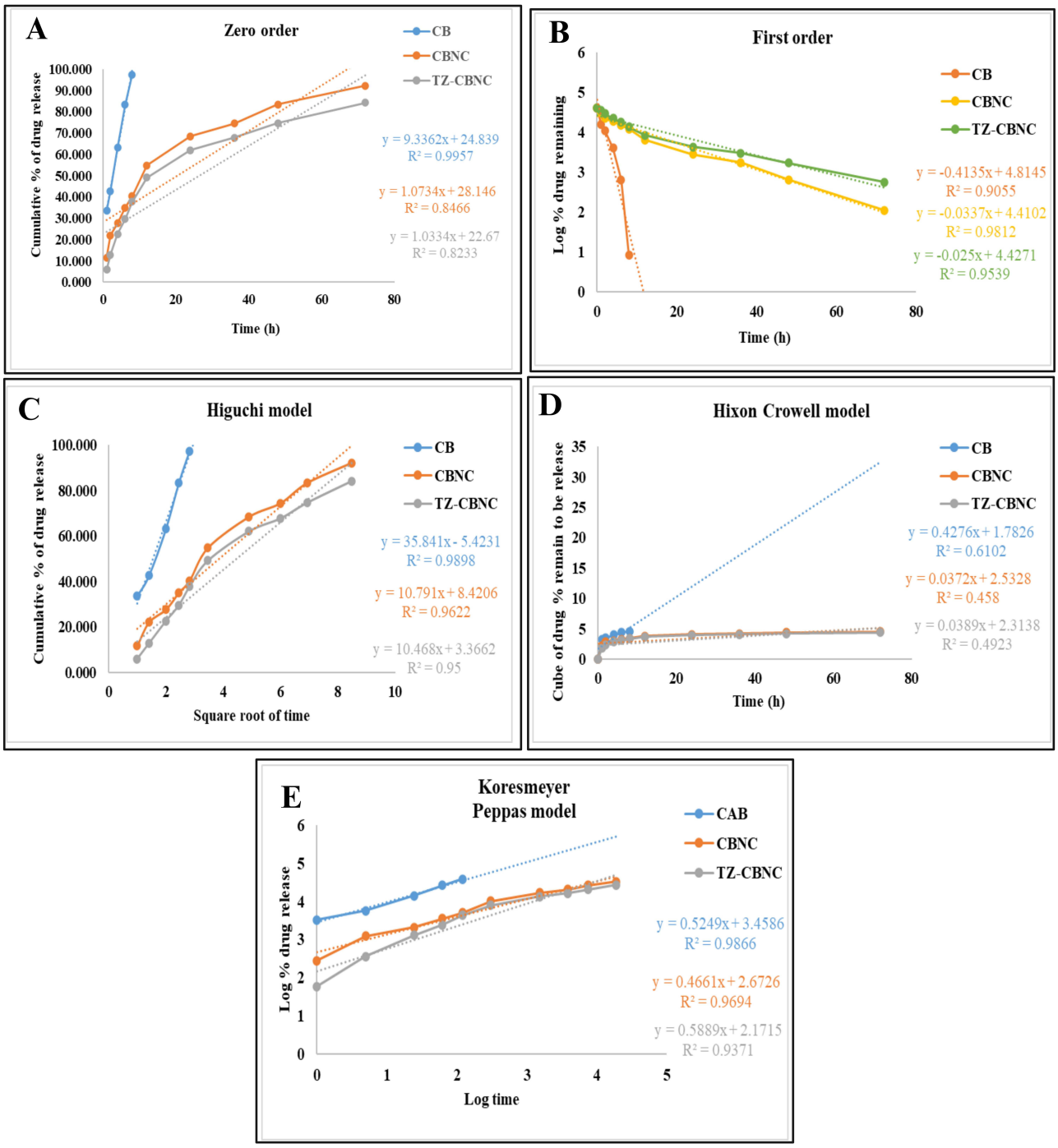

Figure 13 Prediction of drug release kinetics from free capecitabine (CB), optimized capecitabine-loaded nanolipid carriers (CBNC), and trastuzumab conjugated capecitabine-loaded nanolipid carriers (TZ-CBNC): (**A**) Zero order, (**B**) First order, (**C**) Higuchi, (**D**) Hixson Crowell, and (**E**) Korsmeyer Peppas.

dependent cellular cytotoxicity, internalization, regulation of the PIK-AKT signaling cascade, and inhibition of HER2-HER2 receptor dimerization.[26]

Numerous studies have shown that the combination of TZ with CB enhances treatment results in patients with HER2-positive metastatic breast cancer. The retrospective analysis of TZ used alongside paclitaxel and CB reported an 81.1% overall response rate, with a median progression-free survival of 14 months, and overall survival reaching 38.4 months.[41] There were not any discernible alterations in overall survival or progression-free survival between the two regimens in randomized Phase

https://doi.org/10.2147/IJN.S541332

Table 5 The Particle Size, Zeta Potential, and Entrapment Efficiency of CBNCs Were Investigated Under Various Temperature Conditions

Temperature	4°C ± 2°C			24°C ± 2°C, 60% RH			37°C ± 2°C, 75% RH		
Parameter	Particle Size (nm)	Zeta Potential (mV)	Entrapment Efficiency (%)	Particle Size (nm)	Zeta Potential (mV)	Entrapment Efficiency (%)	Particle Size (nm)	Zeta Potential (mV)	Entrapment Efficiency (%)
Initial	194.6	−25.55	79.8	194.6	−25.55	79.8	194.6	−25.55	79.8
1 month	195.3	−25.43	79.3	197.1	−24.56	77.42	202.0	−24.44	76.23
2 months	196.9	−25.17	78.14	200.7	−24.29	76.75	210.6	−23.45	75.34
3 months	205	−24.78	78.57	207.4	−23.67	76.23	217.8	−22.90	73.72

II trial comparing TZ plus CB to lapatinib plus CB, suggesting that no significant differences in progression-free survival or overall survival exist between the two regimens, indicating that TZ plus CB is a therapeutic option.[42]

While nano-sized CB-loaded formulations are employed to address various forms of malignancies, including breast melanoma, they are not sufficiently selective and specific, which leads to off-target effects. Currently, nanotechnology is a fantastic approach for drug transport and is often employed to transport gene treatments and chemotherapeutic drugs to preferred target locations in many diseases, including cancer. Monoclonal antibodies and other ligands that target certain cell receptors can help to transport aggressive anticancer medication and gene therapies to specific tumor locations, cutting costs and limiting excruciating side effects. Using nanocarriers also offers two advantages: a successful distribution of gene therapies to tumor cells and the safeguarding against degradation in the systemic circulation. In order to treat HER2-positive breast cancer, people have tried to make multipurpose NCs with CB and TZ.[26] The study successfully developed TZ-CBNCs for the targeted therapy of HER2-positive breast cancer. The optimized formulation, obtained through the Box-Behnken design, resulted in NCs with an average particle size of 194.6 nm, a high entrapment efficiency of 79.8%, and a drug loading of 8.5%. These characteristics are necessary for successful drug delivery, ensuring stability, uniformity, and better retention at the tumor location due to the enhanced permeability and retention (EPR) effect. The conjugation of TZ increased the particle size to 262 nm. The experimental formulations exhibited a zeta potential of –57.76 mV, indicating enhanced electrostatic repulsion between vesicles, which helps maintain dispersion stability. Evidence supports the idea that a zeta potential outside the range of −30 mV to +30 mV is considered important for achieving stable colloidal suspensions, as it prevents particle aggregation through sufficient repulsive forces.[43,44] It also indicates successful antibody conjugation and enhanced colloidal stability.

FTIR results showed no significant chemical interaction was detected between CB and the excipients, nevertheless, small peak shifts indicated some level of physical interaction. Moreover, a comparison study of the FTIR spectra verified the effective conjugation of TZ to CB-loaded NCs by means of the detection of distinctive amide bond peaks, thereby suggesting protein attachment. According to DSC and XRD examination, encapsulation improved the solubility and stability of CB by converting it into an amorphous state. Again, FESEM pictures revealed an irregular surface for TZ-CBNCs, whereas they had a smooth surface before. The uneven surface of TZ-CBNCs was further validated by means of AFM pictures. According to HR-TEM observations, drug particles appear to be uniformly and densely distributed in the polymer matrix. The surfaces of NCs that were not conjugated were smooth and round, while the surfaces of NCs that had been conjugated with TZ were slightly rougher because of the antibody conjugation. EDX study reveals that the presence of nitrogen increased and the additional presence of sulfur in TZ-CBNCs, which confirms the conjugation of TZ in the antibody-conjugated formulation.

BCA protein assay evidenced successful conjugation of TZ over CBNCs. Qualitative confirmation via SDS-PAGE further demonstrated that the antibody retained its structural integrity and characteristic migration pattern after conjugation. These results collectively supported FTIR and EDX data regarding the successful attachment of TZ through EDC-NHS chemistry to the CBNCs' surface without compromising its functional properties.

In vitro drug release studies indicated that TZ-CBNCs had the slowest and most controlled release profile, which may enhance therapeutic outcomes through sustained drug release and improved bioavailability.[45] The analysis of release

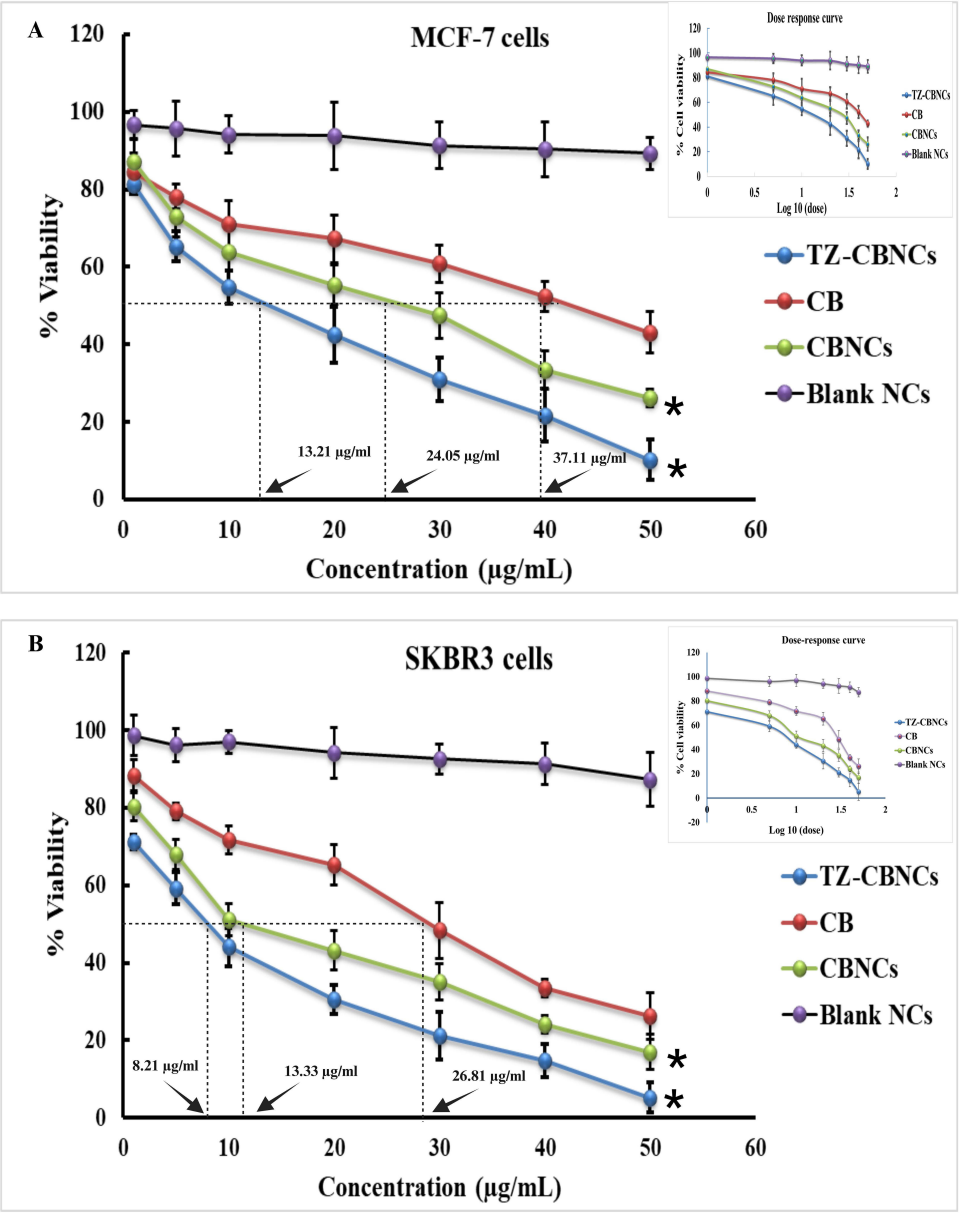

Figure 14 In-vitro cytotoxicity data of free capecitabine (CB), capecitabine-loaded nanolipid carriers (CBNCs), and trastuzumab-conjugated capecitabine-loaded nanolipid carriers (TZ-CBNCs) determined on (**A**) MCF-7 cells and (**B**) SKBR3 cells. Data are presented as mean ± SD (n = 3). Statistical significance was determined at $p < 0.05$ (*), comparing TZ-CBNCs with other treatment groups.

kinetics reveals that CB followed zero-order and CBNC, and TZ-CBNC followed first-order kinetics, implying a concentration-dependent release characteristic of NC systems. High R^2 values in the Korsmeyer-Peppas and Higuchi models supported that the diffusion was the main release mechanism.[46] The slightly decreased R^2 values in TZ-CBNC relative to CBNC may result from steric effects associated with trastuzumab conjugation, potentially affecting surface characteristics and diffusion pathways.[47] The inadequate applicability of the Hixson-Crowell model to all formulations suggests that erosion or alterations in surface area are negligible. TZ conjugation marginally influences but does not modify the release mechanism, hence recommending a controlled and prolonged release appropriate for targeted HER2-positive breast cancer treatment. An "n" value of 0.45 or below indicates Fickian diffusion in the Korsmeyer-Peppas model. In contrast, a "n" value more than 0.45 but less than one signifies non-Fickian diffusion or anomalous transport. An "n" number of one signifies case-I transport, but a "n" value over one denotes super case-II transport as the release mechanism. In our case, the free drug as well as all the tested formulations (CBNC and TZ-CBNC) n value is ranges

https://doi.org/10.2147/IJN.S541332

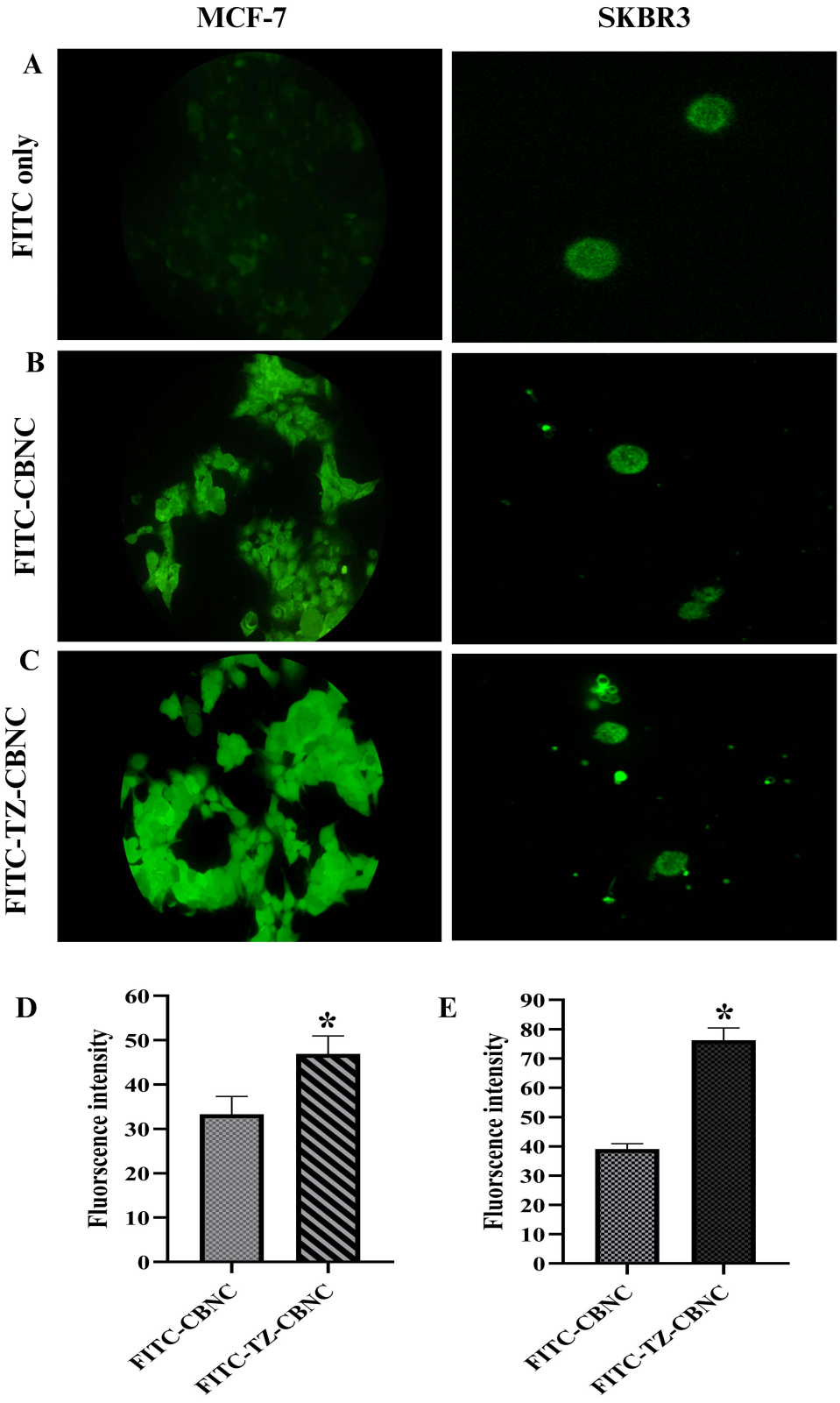

Figure 15 Cellular uptake analysis of Fluorescein Isothiocyanate (FITC) loaded nanolipid carriers (NCs). (**A**) Fluorescein Isothiocyanate (FITC) only, (**B**) Fluorescein isothiocyanate-labeled capecitabine-loaded nanolipid carriers (FITC-CBNCs) at a concentration of 100 ng/mL for 1 hour, and (**C**) Fluorescein isothiocyanate-labeled trastuzumab-conjugated capecitabine-loaded nanolipid carriers (FITC-TZ-CBNCs) at a concentration of 100 ng/mL for 1 hour. (**D**) Fluorescence intensity of FITC-CBNCs and FITC-TZ-CBNCs on MCF-7 cells and (**E**) fluorescence intensity of FITC-CBNCs and FITC-TZ-CBNCs on SKBR3 cells. Statistical significance was determined at $p < 0.05$ (*), comparing FITC-TZ-CBNCs with FITC-CBNCs.

between 0.4461 and 0.588, exhibited all non-Fickian (anomalous) transport, suggesting a combined mechanism of diffusion and polymer relaxation. This behaviour is attributed to the water solubility of the drug and the dynamic nature of the NCs.[48] The diffusion of a hydrophilic drug through the phospholipid bilayer, along with structural reorganisation, swelling of the lipid membrane under physiological conditions, likely contributed to the anomalous transport observed.

The stability data showed that the CBNC formulation exhibited the highest level of stability at refrigerated conditions (4°C), as seen by minimal particle size variation, consistent zeta potential, and maintained entrapment efficiency. A gradual rise in particle size and a decrease in encapsulation efficiency at increased temperatures indicate the emergence of physical instability, potentially attributable to vesicle fusion or drug leakage. The lowering pattern in zeta potential, especially at 37°C, suggests a decrease in electrostatic repulsion, hence heightening the probability of vesicle aggregation. These findings correspond with the colloidal properties of NCs, wherein reduced temperatures facilitate the preservation of bilayer integrity and drug retention.[49] Storage at 4°C is recommended for preserving the physicochemical stability of CBNCs, hence ensuring its effectiveness in targeted HER2-positive breast cancer treatment.

The encapsulated medication was delivered to the cytosol by endocytosis, which absorbed TZ-CBNCs/CBNCs and may occur after endosomal escape.[50] Usually, a greater intracellular distribution of the NCs indicates the effectiveness of encapsulated CB. As a result, a smaller dose may be suitable for exerting a more substantial cytotoxic impact than the free drug. Compared to CBNCs, TZ-CBNCs were more cytotoxic to MCF-7 cells. Further, the cytotoxicity of TZ-CBNCs was found to be maximised against the SKBR3 cell line. We have used two cell lines, MCF-7 (characterized by relatively low HER2 expression) and SKBR3 (with higher HER2 expression), to compare the targeting capability of TZ conjugation. As TZ selectively targets HER2-overexpressing cells, a relatively lower IC_{50} was observed for TZ-CBNCs on SKBR3 cells than on MCF-7 cells. In view of HER2 overexpression in SKBR3 cells, TZ conjugation might drive CBNCs to internalize substantially into the cancer cells. This active targeting might cause prolonged drug release, leading to persistent toxicity, cell cycle arrest, and apoptosis.

Fluorescence microscopy revealed that TZ-functionalized CBNCs were taken up more efficiently than non-conjugated CBNCs in both MCF-7 (HER2-low) and SKBR3 (HER2-high) cells, with the uptake being markedly higher in SKBR3, reflecting the contribution of HER2-mediated internalization. The observed outcomes underscore the potential of this new formulation to enhance the specificity and efficacy of CB in treating HER2-positive breast cancer while reducing off-target effects. Future research on in vivo pharmacokinetics, biodistribution, therapeutic efficacy, and safety will be crucial for translating this targeted drug delivery system into clinical practice. This research provides a strong basis for future studies into targeted nanocarrier therapies for aggressive subtypes of breast cancer.

Conclusion

This study reported the development of TZ-CBNCs as an active targeting strategy towards HER2-positive breast cancer. The strategy overall incorporates the targeting capability of TZ with the chemotherapeutic effectiveness of CB, aiming towards improved drug delivery, surmounting resistance, and improving clinical results. The optimized CBNCs showed favourable physicochemical properties in terms of nano size, spherical shape, surface texture, negative surface charge, and satisfied entrapment efficiency (79.8%) with a sustained CB release profile. TZ conjugation did not affect the surface morphology or size significantly. The optimized CBNCs were stable under recommended storage conditions, highlighting good formulation characteristics towards scalable production. Successful TZ conjugation was substantiated from SDS-PAGE study. TZ-CBNCs were more cytotoxic than CBNCs and free CB against MCF-7 and SKBR3 cells. Sufficient internalization of the tested formulations further supported the in vitro cytotoxic result. The results overall suggested that the TZ-CBNCs may boost the efficiency of chemotherapy while lowering adverse impacts on non-target tissues, making it a promising targeted drug delivery system for HER2-positive breast cancer. However, to establish clinical viability of the experimental TZ-CBNCs, in vivo studies related to pharmacokinetics, biodistribution, safety, and therapeutic efficacy are highly warranted.

Ethical Approval

No animals or humans were involved in this work and hence no need of ethical approval.

Acknowledgments

The authors extend their sincere appreciation to the Deanship of Research and Graduate Studies at King Khalid University for funding this work through Large Research Group. Project number RGP.2/233/46. Furthermore, Dr. Laxmkanta Acharya, Professor, CBT, Faculty of Pharmaceutical Science, Siksha' O' Anusandhan University, Bhubaneswar, is also acknowledged for his contribution to the work.

Funding

The authors extend their sincere appreciation to the Deanship of Research and Graduate Studies at King Khalid University for funding this work through Large Research Group. Project number RGP.2/233/46.

Disclosure

The authors declare that they have no known competing financial interests or personal relationships that could have appeared to influence the work reported in this paper.

References

1. Hani U, Rahamathulla M, Osmani RA, et al. Recent advances in novel drug delivery systems and approaches for management of breast cancer: a comprehensive review. *J Drug Deliv Sci Technol*. 2020;56:101505. doi:10.1016/j.jddst.2020.101505
2. Mondal L, Mukherjee B, Das K, et al. CD-340 functionalized doxorubicin-loaded nanoparticle induces apoptosis and reduces tumor volume along with drug-related cardiotoxicity in mice. *Int J Nanomed*. 2019:8073–8094. doi:10.2147/IJN.S220740
3. Rahamathulla M, Alshahrani SM, Al Saqr A, Alshetaili A, Shakeel F. Effervescent floating matrix tablets of a novel anti-cancer drug neratinib for breast cancer treatment. *J Drug Deliv Sci Technol*. 2021;66:102788. doi:10.1016/j.jddst.2021.102788
4. Kunte S, Abraham J, Montero AJ. Novel HER2–targeted therapies for HER2–positive metastatic breast cancer. *Cancer*. 2020;126(19):4278–4288. doi:10.1002/cncr.33102
5. Waks AG, Winer EP. Breast cancer treatment: a review. *JAMA*. 2019;321(3):288–300. doi:10.1001/jama.2018.19323
6. Peer D, Karp JM, Hong S, Farokhzad OC, Margalit R, Langer R. Nanocarriers as an emerging platform for cancer therapy. *Nano-Enabled Med*. 2020;61–91. doi:10.1038/nnano.2007.387
7. Singh MK, Pindiprolu SK, Sanapalli BK, Yele V, Ganesh GN. Tumor homing peptide modified liposomes of capecitabine for improved apoptotic activity and HER2 targeted therapy in breast cancer: in vitro studies. *RSC Adv*. 2019;9(43):24987–24994. doi:10.1039/c9ra04814f
8. Derakhshani A, Rezaei Z, Safarpour H, et al. Overcoming trastuzumab resistance in HER2-positive breast cancer using combination therapy. *J Cell Physiol*. 2020;235(4):3142–3156. doi:10.1002/jcp.29216
9. Swain SM, Shastry M, Hamilton E. Targeting HER2-positive breast cancer: advances and future directions. *Nat Rev*. 2023;22(2):101–126. doi:10.1038/s41573-022-00579-0
10. Schlam I, Tarantino P, Tolaney SM. Overcoming resistance to HER2-directed therapies in breast cancer. *Cancers*. 2022;14(16):3996. doi:10.3390/cancers14163996
11. Kusumastuti R, Kumagai Y, Ishihara S, et al. Mammaglobin 1 mediates progression of trastuzumab-resistant breast cancer cells through regulation of cyclins and NF-κB. *FEBS Open Bio*. 2022;12(10):1797–1813. doi:10.1002/2211-5463.13468
12. Kumar S, Das S, Sun J, et al. Viswakarma N, Ganesh BB, Duan L. Mixed lineage kinase 3 and CD70 cooperation sensitize trastuzumab-resistant HER2+ breast cancer by ceramide-loaded nanoparticles. *Proc Natl Acad Sci*. 2022;119(38):e2205454119. doi:10.1073/pnas.2205454119
13. Ishida T, Kiba T, Takeda M, et al. Phase II study of capecitabine and trastuzumab combination chemotherapy in patients with HER2 overexpressing metastatic breast cancers resistant to both anthracyclines and taxanes. *Cancer Chemother Pharmacol*. 2009;64:361–369. doi:10.1007/s00280-008-0882-8
14. Yin W, Pei G, Liu G, Huang L, Gao S, Feng X. Efficacy and safety of capecitabine-based first-line chemotherapy in advanced or metastatic breast cancer: a meta-analysis of randomised controlled trials. *Oncotarget*. 2015;6(36):39365. doi:10.18632/oncotarget.5460
15. Murthy RK, Loi S, Okines A, et al. Tucatinib, trastuzumab, and capecitabine for HER2-positive metastatic breast cancer. *N Engl J Med*. 2020;382(7):597–609. doi:10.1056/NEJMoa1914609
16. Mukherjee B, S Satapathy B, Mondal L, S Dey N, Maji R. Potentials and challenges of active targeting at the tumor cells by engineered polymeric nanoparticles. *Curr Pharm Biotechnol*. 2013;14(15):1250–1263. doi:10.2174/13892010156661406081432 35
17. Zhao Z, Ma X, Zhang R, et al. A novel liposome-polymer hybrid nanoparticles delivering a multi-epitope self-replication DNA vaccine and its preliminary immune evaluation in experimental animals. *Nanomedicine*. 2021;35. 102338. doi:10.1016/j.nano.2020.102338
18. Hamelmann NM, Paats JW, Paulusse JM. Cytosolic delivery of single-chain polymer nanoparticles. *ACS Macro Lett*. 2021;10(11):1443–1449. doi:10.1021/acsmacrolett.1c00558
19. Du J, Zong L, Li M, et al. Two-pronged anti-tumor therapy by a new polymer-paclitaxel conjugate micelle with an anti-multidrug resistance effect. *Int J Nanomed*. 2022:1323–1341. doi:10.2147/IJN.S348598
20. Costa D, Santo D, Domingues C, Veiga F, Faneca H, Figueiras A. Recent advances in peptide-targeted micelleplexes: current developments and future perspectives. *Int J Pharm*. 2021;597:120362. doi:10.1016/j.ijpharm.2021.120362
21. Chen F, Li Y, Lin X, Qiu H, Yin S. Polymeric systems containing supramolecular coordination complexes for drug delivery. *Polymers*. 2021;13(3):370. doi:10.3390/polym13030370
22. Zhu Y, Liang J, Gao C, et al. Multifunctional ginsenoside Rg3-based liposomes for glioma targeting therapy. *J Control Release*. 2021;330:641–657. doi:10.1016/j.jconrel.2020.12.036

23. Kenchegowda M, Rahamathulla M, Hani U, et al. Smart nanocarriers as an emerging platform for cancer therapy: a review. *Molecules*. 2022;27(1):146. doi:10.3390/molecules27010146
24. Bazak R, Houri M, El Achy S, Kamel S, Refaat T. Cancer active targeting by nanoparticles: a comprehensive review of literature. *J Cancer Res Clin Oncol*. 2015;141:769–784. doi:10.1007/s00432-014-1767-3
25. Singh MK, Pindiprolu SK, Sanapalli BK, Yele V, Ganesh GN. HER2 targeted biological macromolecule modified liposomes for improved efficacy of capecitabine in breast cancer. *Int J Biol Macromol*. 2020;150:631–636. doi:10.1016/j.ijbiomac.2020.02.131
26. Kumar G, Mullick P, Andugulapati SB, et al. Trastuzumab-conjugated liposomes for co-delivery of paclitaxel and anti-abcb1 siRNA in HER2-positive breast cancer: in vitro and in vivo evaluations. *J Drug Deliv Sci Technol*. 2024;95. 105614. doi:10.1016/j.jddst.2024.105614
27. Alik Kumar L, Pattnaik G, Satapathy BS, et al. Preparation and optimization of gemcitabine loaded PLGA nanoparticle using box-behnken design for targeting to brain: in vitro characterization, cytotoxicity and apoptosis study. *Curr Nanomater*. 2024;9(4):324–338. doi:10.2174/0124054615274558231011164603
28. As KM, Angolkar M, Rahamathulla M, et al. Box-behnken design-based optimization and evaluation of lipid-based nano drug delivery system for brain targeting of bromocriptine. *Pharmaceuticals*. 2024;17(6):720. doi:10.3390/ph17060720
29. Satapathy BS, Mukherjee B, Baishya R, Debnath MC, Dey NS, Maji R. Lipid nanocarrier-based transport of docetaxel across the blood brain barrier. *RSC Adv*. 2016;6(88):85261–85274. doi:10.1039/C6RA16426A
30. Varshosaz J, Ghassami E, Noorbakhsh A, Minaiyan M, Jahanian-Najafabadi A. Trastuzumab-conjugated nanoparticles composed of poly (butylene adipate-co-butylene terephthalate) prepared by electrospraying technique for targeted delivery of docetaxel. *IET Nanobiotechnol*. 2019;13(8):829–833. doi:10.1049/iet-nbt.2018.5363
31. Müller L, Rubio-Pérez G, Bach A, Muñoz-Rujas N, Aguilar F, Worlitschek J. Consistent DSC and TGA methodology as basis for the measurement and comparison of thermo-physical properties of phase change materials. *Materials*. 2020;13(20):4486. doi:10.3390/ma13204486
32. Chauhan A, Chauhan P. Powder XRD technique and its applications in science and technology. *J Anal Bioanal Tech*. 2014;5(5):1–5. doi:10.4172/2155-9872.1000212
33. Satapathy BS, Biswal B, Pattnaik S, Parida R, Sahoo RN. A mucoadhesive nanolipo gel containing Aegle marmelos gum to enhance transdermal effectiveness of linezolid for vaginal infection: in vitro evaluation, in vitro-ex vivo correlation, pharmacokinetic studies. *Int J Pharm*. 2023;648:123542. doi:10.1016/j.ijpharm.2023.123542
34. Satapathy BS, Kumar LA, Pattnaik G, Barik B. Lomustine incorporated lipid nanostructures demonstrated preferential anticancer properties in C6 glioma cell lines with enhanced pharmacokinetic profile in mice. *Acta Chim Slov*. 2021;68(4). doi:10.17344/acsi.2021.6977
35. Arjmand O, Ardjmand M, Amani AM, Eikani MH. Effective adsorption of doxorubicin hydrochloride on green magnetic/graphene oxide/chitosan/allium sativum/quercus/nanocomposite. *Acta Chim Slov*. 2020;67(2):496–506. doi:10.17344/acsi.2019.5513
36. Buddhadev SS, Garala KC, Rahamathulla M, et al. Design, characterization, and evaluation of solid-Self-Nano-Emulsifying drug delivery of benidipine with telmisartan: quality by design approach. *ACS Omega*. 2025;10(16):16440–16456. doi:10.1021/acsomega.4c10838
37. Rahamathulla M, Pokale R, Al-Ebini Y, et al. Simvastatin-encapsulated topical liposomal gel for augmented wound healing: optimization using the box-behnken model. *Evaluations vivo Studies Pharmaceuticals*. 2024;17(6):697. doi:10.3390/ph17060697
38. Sethy C, Kundu CN. 5-Fluorouracil (5-FU) resistance and the new strategy to enhance the sensitivity against cancer: implication of DNA repair inhibition. *Biomed Pharmacother*. 2021;137:111285. doi:10.1016/j.biopha.2021.111285
39. Freudenberg JA, Wang Q, Katsumata M, Drebin J, Nagatomo I, Greene MI. The role of HER2 in early breast cancer metastasis and the origins of resistance to HER2-targeted therapies. *Exp Mol Pathol*. 2009;87(1):1. doi:10.1016/j.yexmp.2009.05.001
40. Iqbal N, Iqbal N. Human epidermal growth factor receptor 2 (HER2) in cancers: overexpression and therapeutic implications. *Mol Biol Int*. 2014;2014(1):852748. doi:10.1155/2014/852748
41. Tonyali O, Benekli M, Berk V, et al. Efficacy and toxicity of Trastuzumab and paclitaxel plus capecitabine in the first-line treatment of HER2-positive metastatic breast cancer. *J Cancer Res Clin Oncol*. 2013;139:981–986. doi:10.1007/s00432-013-1409-1
42. Takano T, Tsurutani J, Takahashi M, et al. A randomized phase II trial of trastuzumab plus capecitabine versus lapatinib plus capecitabine in patients with HER2-positive metastatic breast cancer previously treated with trastuzumab and taxanes: WJOG6110B/ELTOP. *Breast*. 2018;40:67–75. doi:10.1016/j.breast.2018.04.010
43. Kocbek P, Obermajer N, Cegnar M, Kos J, Kristl J. Targeting cancer cells using PLGA nanoparticles surface modified with monoclonal antibody. *J Control Release*. 2007;120(1–2):18–26. doi:10.1016/j.jconrel.2007.03.012
44. Sahoo SK, Labhasetwar V. Enhanced antiproliferative activity of transferrin-conjugated paclitaxel-loaded nanoparticles is mediated via sustained intracellular drug retention. *Mol Pharm*. 2005;2(5):373–383. doi:10.1021/mp050032z
45. Honmane SM, Chimane SM, Bandgar SA, Patil SS. Development and optimization of capecitabine loaded nanoliposomal system for cancer delivery. *Indian J Pharm Edu Res*. 2020;54:376–384. doi:10.5530/ijper.54.2.4
46. Rahamathulla M, Hv G, Veerapu G, et al. Characterization, optimization, in vitro and in vivo evaluation of simvastatin proliposomes, as a drug delivery. *AAPS Pharm Sci Tech*. 2020;21(4):129. doi:10.1208/s12249-020-01666-4
47. Du J, Liu X, Sun J, et al. Trastuzumab-functionalized bionic pyrotinib liposomes for targeted therapy of HER2-positive breast cancer. *Breast Cancer Res*. 2024;26(1):99. doi:10.1186/s13058-024-01853-2
48. Wu KW, Sweeney C, Dudhipala N, et al. Primaquine loaded solid lipid nanoparticles (SLN), nanostructured lipid carriers (NLC), and nanoemulsion (NE): effect of lipid matrix and surfactant on drug entrapment, in vitro release, and ex vivo hemolysis. *AAPS Pharm Sci Tech*. 2021;22(7):240. doi:10.1208/s12249-021-02108-5
49. Taira MC, Chiaramoni NS, Pecuch KM, Alonso-Romanowski S. Stability of liposomal formulations in physiological conditions for oral drug delivery. *Drug Deliv*. 2004;11(2):123–128. doi:10.1080/10717540490280769
50. Romond EH, Perez EA, Bryant J, et al. Trastuzumab plus adjuvant chemotherapy for operable HER2-positive breast cancer. *N Engl J Med*. 2005;353(16):1673–1684. doi:10.1056/NEJMoa052122